# Reactive Metabolites from Thiazole-containing Drugs: Quantum Chemical Insights into Biotransformation and Toxicity

Chaitanya K. Jaladanki,[1] Samima Khatun,[1] Holger Gohlke,[2,3] Prasad V. Bharatam[1*]

[1]*Department of Medicinal Chemistry, National Institute of Pharmaceutical Education and Research (NIPER), Sector - 67, S. A. S. Nagar (Mohali), 160 062 Punjab, India.*

[2]*Heinrich-Heine-Universität Düsseldorf, Institut für Pharmazeutische und Medizinische Chemie, Universitätsstr. 1, 40225 Düsseldorf, Germany*

[3]*Forschungszentrum Jülich GmbH, John von Neumann Institute for Computing (NIC), Jülich Supercomputing Centre (JSC), and Institute of Biological Information Processing (IBI-7: Structural Biochemistry), Wilhelm-Johnen-Straße, 52425 Jülich, Germany*

*Corresponding Author

Prof. Prasad V. Bharatam
Department of Medicinal Chemistry
National Institute of Pharmaceutical Education and Research (NIPER),
Sector – 67, S. A. S. Nagar (Mohali), 160 062
Punjab, India
Telephone: +91 172 2292018; Fax: +91 172 2214692.
E-mail: pvbharatam@niper.ac.in

**”FOR TABLE OF CONTENTS ONLY”**

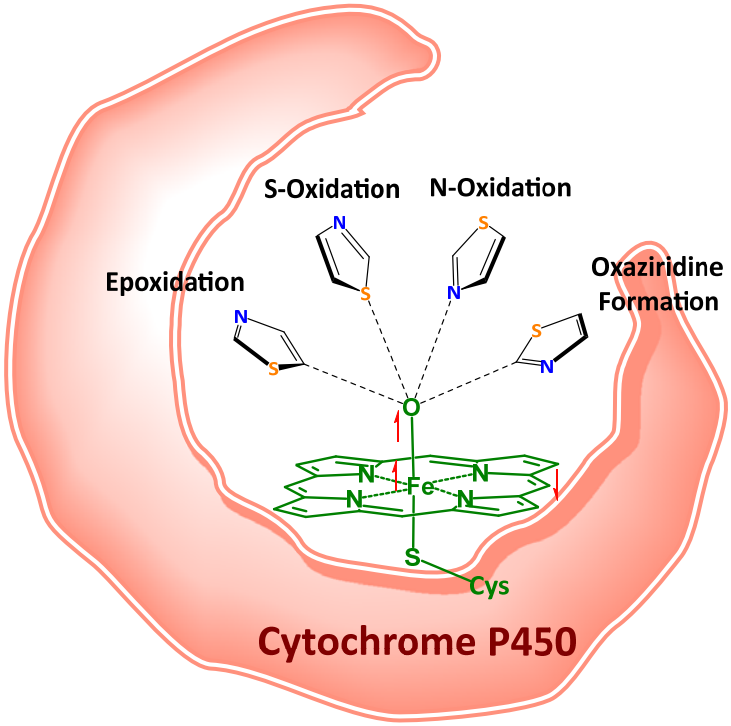

## Abstract

Drugs containing thiazole and aminothiazole groups are known to generate reactive metabolites (RMs) catalyzed by cytochrome P450s (CYPs). These RMs can covalently modify essential cellular macromolecules and lead to toxicity and induce idiosyncratic adverse drug reactions. Molecular docking and quantum chemical hybrid DFT study were carried out to explore the molecular mechanisms involved in the biotransformation of thiazole (TZ) and aminothiazole (ATZ) groups leading to RMs epoxide, *S*-oxide, *N*-oxide, and oxaziridine. The energy barrier required for the epoxidation is 13.63 kcal/mol, that is lower than that of *S*-oxidation, *N*-oxidation and oxaziridine formation, (14.56, 17.90, and 20.20, kcal/mol respectively). The presence of the amino group in ATZ further facilitates all the metabolic pathways, for example, the barrier for the epoxidation reaction is reduced by ~2.5 kcal/mol. Some of the RMs/their isomers are highly electrophilic and tend to form covalent bonds with nucleophilic amino acids, finally leading to the formation of metabolic intermediate complexes (MICs). The energy profiles of these competitive pathways have also been explored.

Keywords: Thiazole, Thiazole epoxide, *S*-oxidation, Cytochrome P450s, Direct oxygen transfer.

## Introduction

Electrophilic reactive metabolites (RMs) may be formed during the biotransformation of drugs, which can covalently modify the cytochrome P450s (CYPs) enzymes or essential cellular macromolecules, that way interfering with biological function and causing drug-drug interactions or idiosyncratic adverse drug reactions.[1–4] Certain chemical functional groups are implicated in the generation of toxic RMs and are declared as structural alerts.[1,5–8] Aromatic five-membered heterocyclic rings such as furan, thiophene, thiazoles, aminothiazoles, and benzothiazoles come under scrutiny because these species can lead to toxicity during biotransformation.[1,5,7,9–12]

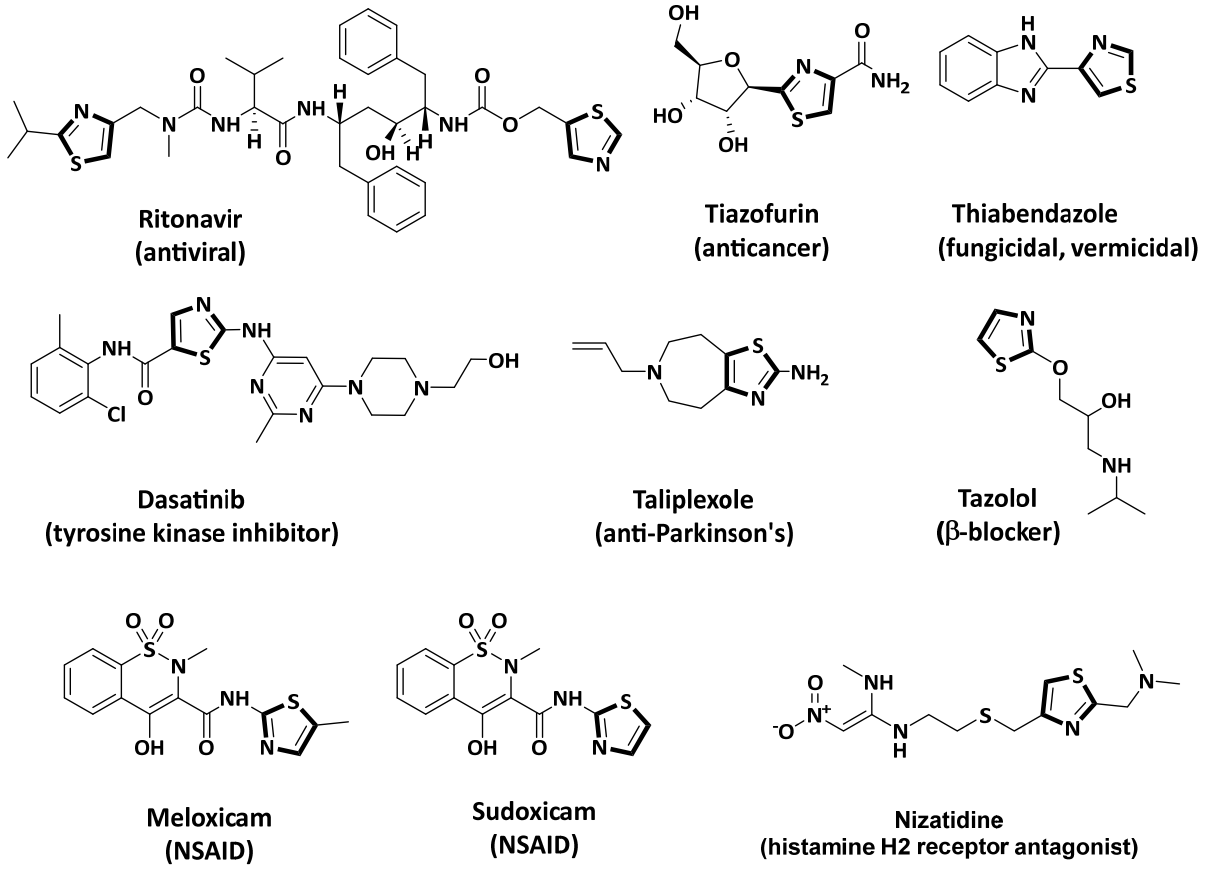


**Figure 1.** A representative list of drugs carrying thiazole functional groups, which are reported to undergo metabolic reactions at the thiazole group.

Compounds carrying thiazole (TZ) and aminothiazole (ATZ) groups gained significant interest in medicinal chemistry, due to their frequent occurrence in many biologically active molecules.[13,14] Figure 1 shows 2D structure of important thiazole ring containing drugs (a comprehensive list is provided in Table S1 and Figure S1, ESI). A wide variety of pharmacological activities (antineoplastic, antidiabetic, anticonvulsant, antimicrobial, and anti-

inflammatory agents) are exhibited by these compounds. A few thiazole containing drugs are also reported for antiviral effects including anti-COVID.[15,16] Thiazole ring is also being considered as a structural alert in drug discovery research. Several thiazole carrying drugs were reported for their toxicity (e.g. sudoxicam, thiabendazole, ritonavir). For instance, sudoxicam undergoes biotransformation by epoxidation followed by a ring-opening reaction, leading to the formation of thioamides, which are known to form covalent adducts.[4,7,17,18]

Mizutani et al. reported the formation of toxic metabolites from thiazole and thiabendazole in mice.[19–21] Kalgutkar and co-workers demonstrated the bioactivation of a 2-amino-4-arylthiazole functional group in human liver microsomes and characterized its GSH adducts using LC–MS/MS and NMR techniques.[22] Lakshmi et al. reported the mechanism for the formation of a thioether conjugate from 2-amino-4-(5-nitro-2-furyl)-thiazole.[23,24] Burnett and co-workers reported the formation of an *N*-oxide-*S*-oxide metabolite from 4,5-dimethyl thiazole.[25] Kalgutkar et al. found that a thrombopoietin receptor agonist with a thiazole ring[22] endured amide hydrolysis followed by the activation of the thiazole ring, which is prone to a nucleophilic attack at $C^5$ centre such that the oxidation of 2-aminothiazole leads to covalent modification of the cytochrome. Subramanian et al. studied the cytochrome-mediated epoxidation of 2-aminothiazole-based AKT inhibitors.[26]

Although the only structural difference between meloxicam and sudoxicam is the presence of an additional methyl group on the C5-position of 2-carboxamidothiazole scaffold in meloxicam, a significant difference in their toxicological profile in humans was noticed.[11,17,27,28] Hobbs and Twomey studied the metabolism of sudoxicam in rat, monkey, dog, and identified thiohydantoic acid and thiourea resulting from thiazole ring scission of sudoxicam using mass spectral analysis.[29] Obach et al. performed *in vitro* metabolism studies on sudoxicam and meloxicam, and reported that the CYP metabolism led to the formation of a thiazole scission product acyl thiourea, which is a protoxin.[17]

The CYPs are membrane-bound proteins, containing heme as a cofactor, which are involved in an oxygen atom transfer to the xenobiotic via a complex catalytic cycle. CYPs are the major oxidizing enzymes in affecting the chemistry of TZ as reported in Figure 2. However, several detailed questions relating to these suggested RMs have not yet been addressed. Figure 2 shows the possible reaction pathways of a TZ ring (mediated by CYPs), which can lead to the biotransformation causing toxic side effects. Although several studies have been carried out to explore the mechanisms leading to toxic products from thiazole-containing compounds using experimental methods, exact details on how cytochrome-mediated toxicity originates from

these species is still missing. To identify the common reaction mechanisms associated with the biotransformation of TZ compounds and to obtain atomic-level details as well as to explore the energy profiles associated with the metabolic reactions, quantum chemical calculations were performed on the model thiazole ring. The four reactions considered in Figure 2 were explored to obtain structures of the intermediates, transition states and metabolic intermediate complexes along the reaction pathways. The energy profiles were established, and the electronic characteristics of all of the species on the reaction pathway were explored. Recently, we reported quantum chemical studies on the Mechanism Based Inhibition (MBI) originating from nitroso,[30] epoxides,[31] *S*-oxide,[32–34] carbene,[35] functional groups by CYPs, which are associated with various drugs. In this study, quantum chemical analyses on the biotransformation of TZ (and ATZ) against Compound I (Cpd I) are reported.

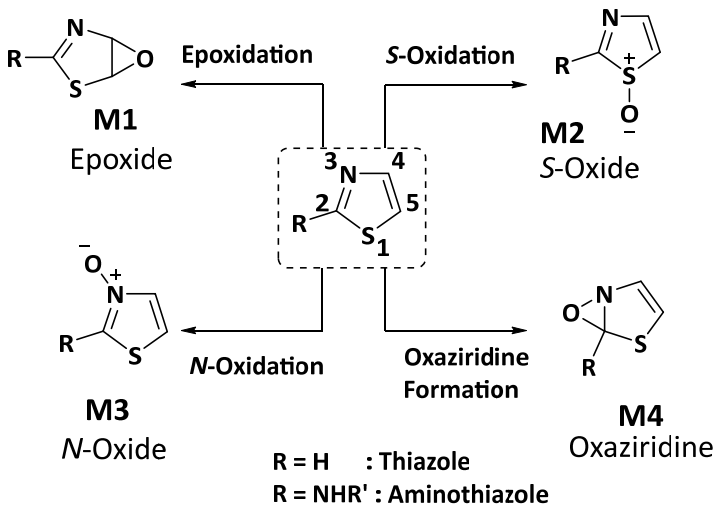


**Figure 2.** The biotransformation pathways reported for drugs carrying thiazole rings.

## METHODS

### Molecular Docking

A library of 120 thiazole ring containing drugs were extracted from the DrugBank database (Table S1, ESI).[36] 84 compounds from this list were subjected to molecular docking based on their molecular mass. The preparation and minimization of the thiazole ring containing compounds were performed using the LigPrep module[37] with the OPLS3e force field.[38] For molecular docking analysis, crystal structures of the CYP3A4 (PDB ID: 5VCC), CYP2C9 (PDB ID: 5A5I), CYP2C19 (PDB ID: 4GQS), CYP2D6 (PDB ID: 3TBG), and CYP2E1 (PDB ID: 3T3Z) with high resolution were utilized. The protein structure of CYP isoforms were preprocessed using Protein Preparation wizard.[39] Hydrogen atoms were added and assigned the right bond orders. An oxygen atom is added to the Fe center of heme group (i.e., Fe(IV) state at the heme center) in the active state and appropriate charges added to Fe, O, N, and S atoms. Then molecular docking studies were performed using Glide software in Schrodinger suite of programs[40] The Receptor Grid Generation module of Glide was used to generate grid for docking purposes, the outer cubical grid was extended up to 20 Å in the vicinity of Fe-porphyrin (active site of CYP's), while maintaining the inner box size at the default value (10 × 10 × 10 $Å^3$). The highest ranked poses were visually inspected and analyzed for their interactions with active site residues as well as with the Fe=O center of the heme. The OPLS3e force field was employed for identifying and ranking the docking poses.

### Quantum Chemical (QC) Methods

Quantum chemical calculations using Gaussian 09 suite of programs, were carried out to understand the metabolism of TZ, ATZ and the covalent adduct formation from the RMs of these species, leading to MBI of CYPs.[41] To mimic CYPs, the model species Cpd I was used as the model oxidant,[42,43] which is an iron (IV-oxo) radical cation with heme-porphine with $SH^-$ at the axial position. This model has been accepted by various scientific groups to provide reasonably accurate energy estimates for CYP-catalyzed metabolic studies.[42–47] For this study, the multi-state reactivity (both doublet and quartet states) of Cpd I was considered. The geometry optimization of all of the intermediates on the metabolic path of TZ leading to MBI were performed using hybrid density functional (DFT) method B3LYP, with a basis set 6-31+G(d) [48–52] (except Fe) and LanL2DZ[53] basis set on the Fe center. The optimization of transition states were performed using a guess initial structure using Berny optimization method. The frequency calculations were carried out using the same method to characterize the

stationary points as minima or transition states (as first-order saddle points with one imaginary vibrational mode). To mimic the polarity of the CYP active site cavity (dielectric constant (ε) = 5.69, close to chlorobenzene), single point calculations were employed using a self-consistent reaction field (SCRF) method IEFPCM (Integral Equation Formalism variant of the Polarizable Continuum Model)[54] at B3LYP/6-311++G(d,p) level on the optimized structures. The absolute energies obtained using this method were further corrected with the gas phase Gibbs energy correction values. The electrophilicity analysis[55,56] was performed to estimate the global and local electrophilicity indices of all important reactive metabolites. The electronegativity (χ), hardness (η), global electrophilicity (ω) and global nucleophilicity (*N*) are calculated using the eq. 1, eq. 2, eq. 3 and eq. 4, respectively. The local Fukui functions for electrophilic ($f_k^+$) and nucleophilic ($f_k^-$) attack using charges on each atom $q_k$ are estimated by eq. 5 and eq. 6. The natural orbital (NBO) population analysis was used for N and N-1 and N+1 number of electrons on the relevant species.The local electrophilicities and local nucleophilicities are estimated by using eq. 7 and eq. 8, respectively. The reliability of the global and local nucleophilicity values to explain the observed chemistry is much weaker than that of global and local electrophilicity values. However, in this particular work it is noted that the results are partially useful (Table 2).

$$\chi = -\frac{\in_{HOMO} + \in_{LUMO}}{2}; \qquad \begin{matrix}\chi = Electronegitivity \\ \in_{HOMO} = Energy\ of\ HOMO\ orbital \\ \in_{LUMO} = Energy\ of\ LUMO\ orbital\end{matrix} \qquad (1)$$

$$\eta = \in_{LUMO} - \in_{HOMO}\ ; \qquad \eta = hardness \qquad (2)$$

$$\omega = \frac{\mu^2}{2\eta} = \frac{\chi^2}{2\eta}\ ; \qquad \omega = Global\ electrophilicity \qquad (3)$$

$$\boldsymbol{N = \frac{1}{\omega}}\ ; \qquad \boldsymbol{N = global\ nucleophilicity} \qquad (\mathbf{4})$$

$$f_k^+ = q_k(\mathrm{N}+1) - q_k(\mathrm{N}); \qquad f_k^+\ is\ Fukui\ function\ for\ nucleophilic\ attack \qquad (5)$$

$$f_k^- = q_k(\mathrm{N}) - q_k(\mathrm{N}-1); \qquad f_k^-\ is\ Fukui\ function\ for\ electrophilic\ attack \qquad (6)$$

$$\omega_k = \omega f_k^+\ ; \qquad \omega_k = local\ electrophilicity \qquad (7)$$

$$N_k = \omega f_k^-\ ; \qquad N_k = local\ electrophilicity \qquad (8)$$

Where, $q_k$ (N), $q_k$ (N+1), $q_k$ (N-1) respectively are partial atomic charges at atom $k$ in neutral, anionic and cationic states of the molecules.

## Results and Discussion

### Site of Metabolism studies using molecular docking analysis

The molecular docking analysis of a library of 84 compounds with a thiazole ring were carried out to identify the preferred site of metabolism (SOM) and orientation at the CYP active site of these compounds, screened against five CYP isoforms CYP3A4, CYP2C9, CYP2C19, CYP2D6 and CYP2E1. Among the 84 ligands chosen, the docking poses of only 52 substrates have shown SOM at the thiazole ring at any of the 4 possible sites, i.e., epoxidation, *S*-oxidation, *N*-oxidation and oxaziridine formation (Table 1).

Based on the highest ranking pose, it can be concluded that the majority of ligands showed SOM at the sulfur atom and the unsaturated center of the thiazole ring. For instance, compounds such as ritonavir,[57,58] cobicistat,[59] and sulfathiazole showed SOM at unsaturated bond of the thiazole ring as their top ranked pose. Cambendazole, pramipexole and famotidine showed SOM at sulfur atom within the active site cavity of CYPs. At the same time, clomethiazole, showed nitrogen atom pointed towards Fe=O, it is known that clomethiazole forms *N*-oxide metabolite in CYP2E1 and CYP3A4.[60,61] A few compounds showed the SOM at both epoxidation and *S*-oxidation sites– e.g. thiabendazole, vosaroxin and varlitinib.

In CYP3A4 and CYP2E1, it is well known that the active site is highly hydrophobic due to six phenylalanine residues (108, 213, 215, 220, 241, and 304), isoleucine (120 and 301), and valine (240) residues in CYP3A4 and five phenylalanine residues (106, 116, 207, 298, and 478) and leucine (210) residues in CYP2E1. The hydrophobic groups are majorly located at the dome region of CYP3A4[62] and CYP2E1,[63] which directs the orientation of thiazole towards the heme Fe=O center. Alternatively, in the case of CYP2C9, the hydrophilic residues arginine and lysine control the docking pose, directing the thiazole ring towards the heme prosthetic group.

The molecular docking analysis showed an overall success rate of the order of 60 %. The individual success rates with reference to each type of reactions of thiazole metabolism reactions are epoxidation (58%), *S*-oxidation (34%), *N*-oxidation (8%) and oxaziridination (0%). These results are indicating that it is possible to distinguish the preferred metabolic reaction of the thiazole containing compounds after successfully predicting the SOM. The molecular docking analysis helps in identifying which enzyme residues govern the orientation of ligand inside the active site rather than nailing down the actual SOM because the possible SOMs are adjacent to each other. These results are only partially satisfactory, incorporating

electronic effects in the study is warranted. Performing Induced Fit docking studies and QM/MM analysis are expected to improve the predictive power. These suggested methods are currently out of reach for routine analysis. Thus, we have taken up detailed quantum chemical analysis on small model systems to estimate the energy profiles along the four oxidation paths (Figure 2).

**Table 1.** Number of thiazole containing substrates which predict preferred oxidation path (using molecular docking analysis) against 5 CYPs. These results are as per the 1st ranked molecular docking pose. Total number of substrate is 84.

| | No. of compounds predicted for metabolic reaction | | | |
|---|---|---|---|---|
| | Epoxidation | *S*-oxidation | *N*-oxidation | Oxaziridine formation |
| CYP3A4 | 48 | 32 | 2 | 2 |
| CYP2C9 | 45 | 35 | 3 | 1 |
| CYP2C19 | 46 | 35 | 1 | 2 |
| CYP2D6 | 41 | 40 | 2 | 1 |
| CYP2E1 | 38 | 44 | 2 | - |

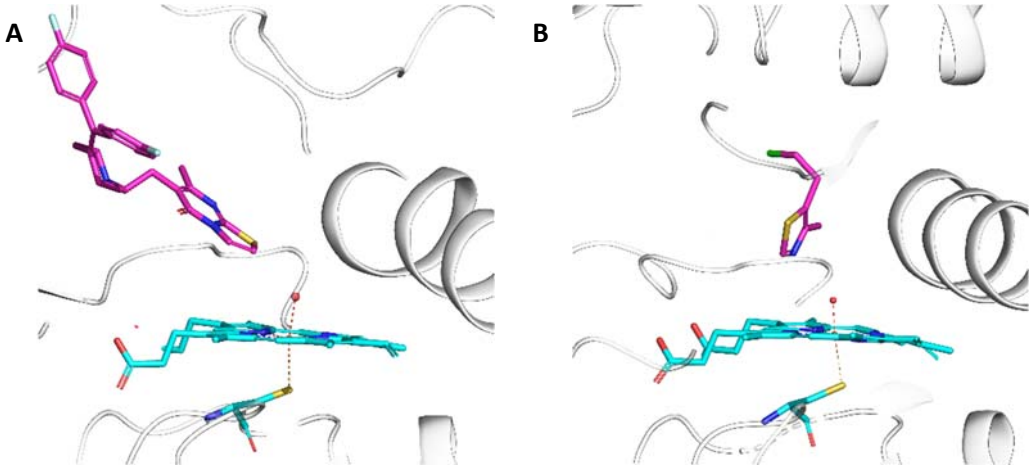


**Figure 3** (A) The docking poses of ritaverin in CYP3A4 active site favouring epoxidation and (B) the docking pose of clomethiazole in the active site of CYP2E1 favoring *N*-oxidation.

## Quantum Chemical Studies

### Formation of reactive metabolites

***Epoxidation :*** Epoxidation is one of the important metabolic reactions in drug molecules containing unsaturated functional units such as alkene,[64–70] and cycloalkene,[71,72] thiophene,[11,34,73–80] furan,[31,81,82] thiazole,[11,17,19,21,83,84] and phenyl.[85] Several experimental and theoretical studies on epoxidation reactions catalyzed by CYPs were reported.[5,9,65–68,83,84,86–88,10,11,26,31,34,47,63,64] Several research groups reported the epoxidation reaction at aliphatic and alicyclic unsaturated centers using quantum chemical methods.[42,65,66,70,89] The mechanism of epoxidation reaction involves two steps, an initial C–O bond formation (via C=C bond activation step) followed by ring closure. In our previous studies, we have elucidated several vital features involved in the epoxidation process of furan[31] and thiophene[34] rings using Cpd I as an oxidant and also investigated the MBI of the epoxide metabolites. The epoxidation of TZ using quantum chemical analysis is highlighted in this section.

The epoxidation reaction happens at the $C^4$=$C^5$ bond of the TZ ring. Since epoxidation involves two distinct phases (C=C activation phase, epoxide formation phase),[66,70,87] the initial nucleophilic attack can happen, in principle, at either $C^4$ or $C^5$. The local nucleophilicity value [55,56] at the $C^5$ center ($N_k^-$= –0.47 eV) is markedly larger than that at the $C^4$ center ($N_k^-$= –0.10 eV) (Table 1). Thus, the reaction pathway has been explored with reference to an initial $S_N2$ reaction originating from the $C^5$ center. In the transition state **$^2$TS-E** (Figure 4), the $C^5$–O distance (1.94 Å) is much shorter than the $C^4$–O distance (2.62 Å). The estimated energy barrier for direct oxygen transfer (DOT) reaction at the $C^5$ center is 13.63 kcal/mol via **$^2$TS-E** on the doublet potential energy surface (PES) (Figure 4) and leads to the formation of intermediate radical complex **$^2$I-E**. For comparison, the energy barrier for the epoxidation of ethene, furan, and thiophene by Cpd I was reported to be 14.90,[66] 12.33,[31] and 15.71 kcal/mol.[34] In **$^2$I-E** complex, the Fe−O interaction (2.54 Å) continues to exist. The epoxide product complex **$^2$PC-E** is 25.42 kcal/mol more stable than the starting species, indicating that the epoxidation reaction is an exergonic and a thermodynamically favorable process. **$^2$PC-E** shows weak Fe=O electrostatic interaction with a distance of 2.37 Å. Breaking of this bond leads to the formation of epoxide metabolite (**M1**), which is endergonic by 1.41 kcal/mol (see ESI, Figure S5, for corresponding energy profile using quartet state of the Cpd I) On the doublet PES, the $S_N2$ reaction progresses due to the transfer of electron density from the $C^4$-$C^5$ π orbital to the π*orbital of the Fe=O bond (Figure 6a).

**-Table 2.** Local nucleophilicity ($N_k^-$) values of TZ and ATZ. The values were obtained using natural population charge analysis.

| Atom | $N_k^-$ of TZ | $N_k^-$ of ATZ |
|---|---|---|
| **S (1)** | 0.11 | 0.18 |
| **C2** | -0.29 | 0.09 |
| **N (3)** | -0.40 | -0.58 |
| **C4** | -0.10 | -0.09 |
| **C5** | -0.47 | -0.60 |

***S-oxidation*:** *S*-oxidation is one of the important reactions in the drug metabolism and detoxification by CYPs in the liver. Studies on *S*-oxidation reactions have been reported extensively using experimental and theoretical approaches and suggested a concerted $S_N2$ mechanism.[90–93] To understand the S-oxidation reaction, quantum chemical exploration was extensively carried out using different model oxidants ($H_2O_2$, HOONO, Cpd I)[32,33,95–104,34,105,43,87,90–94] on a wide range of aliphatic sulfides that differ in the length of the alkyl chain and ranging from a hydrogen atom to an ethyl group,[43,94,96,97,104–106] cyclic sulfides,[32,33] and aromatic sulfides.[34]

Structure **$^2$TS-S** (Figure 4) represents the transition state of the *S*-oxidation reaction modelled with TZ with Cpd I. In **$^2$TS-S**, the S–O bond length is 2.06 Å, which is slightly smaller than the reported value on dimethyl sulfide (2.22 Å),[98] thiazolidinedione (2.16 Å),[32] and thiophene (2.15 Å).[34] The energy barrier required for the *S*-oxidation reaction in TZ is 17.90 kcal/mol via transition state **$^2$TS-S** (Figure 5). This barrier is higher than that for the reaction of thiophene (14.75 kcal/mol) [34] and thiazolidinedione (11.59 kcal/mol).[32] In the product complex **$^2$PC-S**, the S=O bond is formed and the Fe–O bond is almost broken. In **$^2$PC-S**, the sulfur atom of sulfoxide metabolite (**M2**) adopts strong pyramidalization (sum of angles around sulfur ~310.8°). The formation of the intermediate $^2$PC-S is favorable by 4.16 kcal/mol on the doublet PES of Cpd I compared to the starting species. Further, **M2** is less stable than **M1** by 24.26 kcal/mol. The MO analysis (Figure 6b) shows the *S*-oxidation in the doublet state is facilitated by the electron density donated preferentially from the *p*-lone pair electrons ($n_S$) of sulfur atom to the $\pi^*_{xz}$ orbital of the Fe–O bond.

***N-oxidation:*** The *N*-oxidation is also an important reaction in drug metabolism to detoxify drugs by CYPs. Several experimental and theoretical studies were reported on *N*-oxidation reactions.[98,107–109] Quantum chemical studies on the mechanism of *N*-oxidation using model oxidant Cpd I were performed extensively for primary,[30,110–114] secondary,[112] and tertiary amines,[98,107–109,115] hydrazine,[110,116,117] and aromatic amines,[112,118,119] and the reported barriers

for *N*-oxidation are in the range of 10-20 kcal/mol. In the case of TZ, the nucleophilicity originating from the N-center is less than that of the $C^5$ center (Table 1). Only a few experimental studies reported *N*-oxidation originating from the TZ ring,[25] in these cases, the structural details of the *N*-oxide metabolites were not provided.

For comparison purposes, quantum chemical studies on the *N*-oxidation pathway were also performed. The *N*-oxidation reaction of TZ leads to the generation of a thiazole-*N*-oxide product (**PC-N**) (Figure 4). The *N*-oxidation process also involves a DOT mechanism, in which an oxygen atom is transferred to the N-center of TZ from Cpd I via a transition state **$^2$TS-N** (Figure 4). This *N*-oxidation reaction process requires an energy barrier of 20.20 kcal/mol on the doublet state PES via **$^2$TS-N** (Figure 5). In the *N*-oxidation reaction, the electron density is donated from the nitrogen lone pair orbital into the $\pi^*$ orbital of Fe–O. In the product complex **$^2$PC-N**, the Fe–O bond is almost broken. **$^2$PC-N** is 16.29 kcal/mol exergonic on the doublet PES of Cpd I. This is also mirrored in the transition state geometries, where early (**$^2$TS-N**) (O–N distance of 1.95 Å) transition state found for the doublet states. The *N*-oxide metabolite **M3** is much less stable than that of **M1** (by 36.02 kcal/mol).

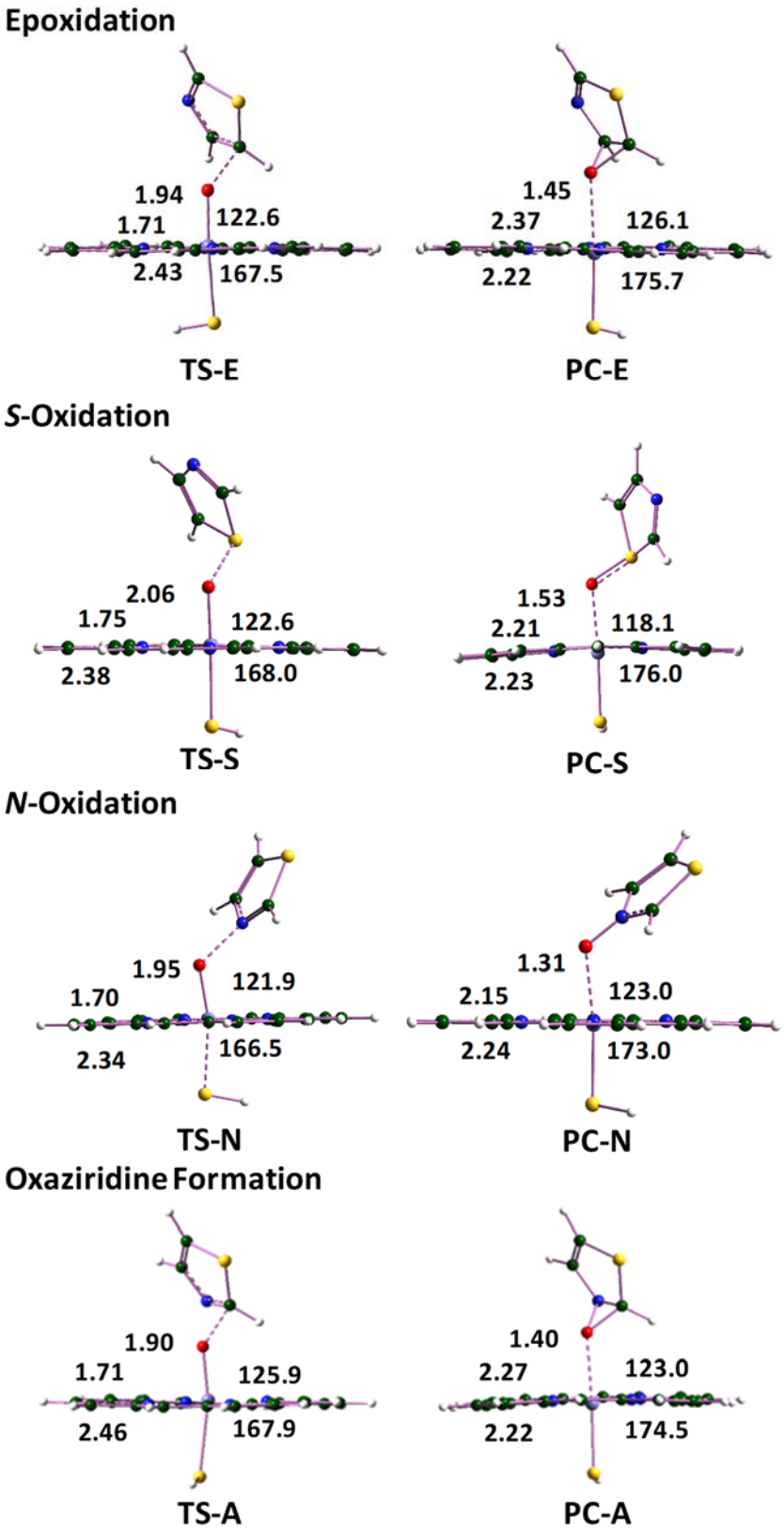


**Figure 4.** Optimized geometries of transition states (**TS-E, TS-S, TS-N, TS-A**) and product complexes (**PC-E, PC-S, PC-N, PC-A**) along the various reaction pathways of thiazole. The values are on the doublet potential energy surface. All bond lengths are in Ångstrom (Å) and bond angles are in degrees (°).

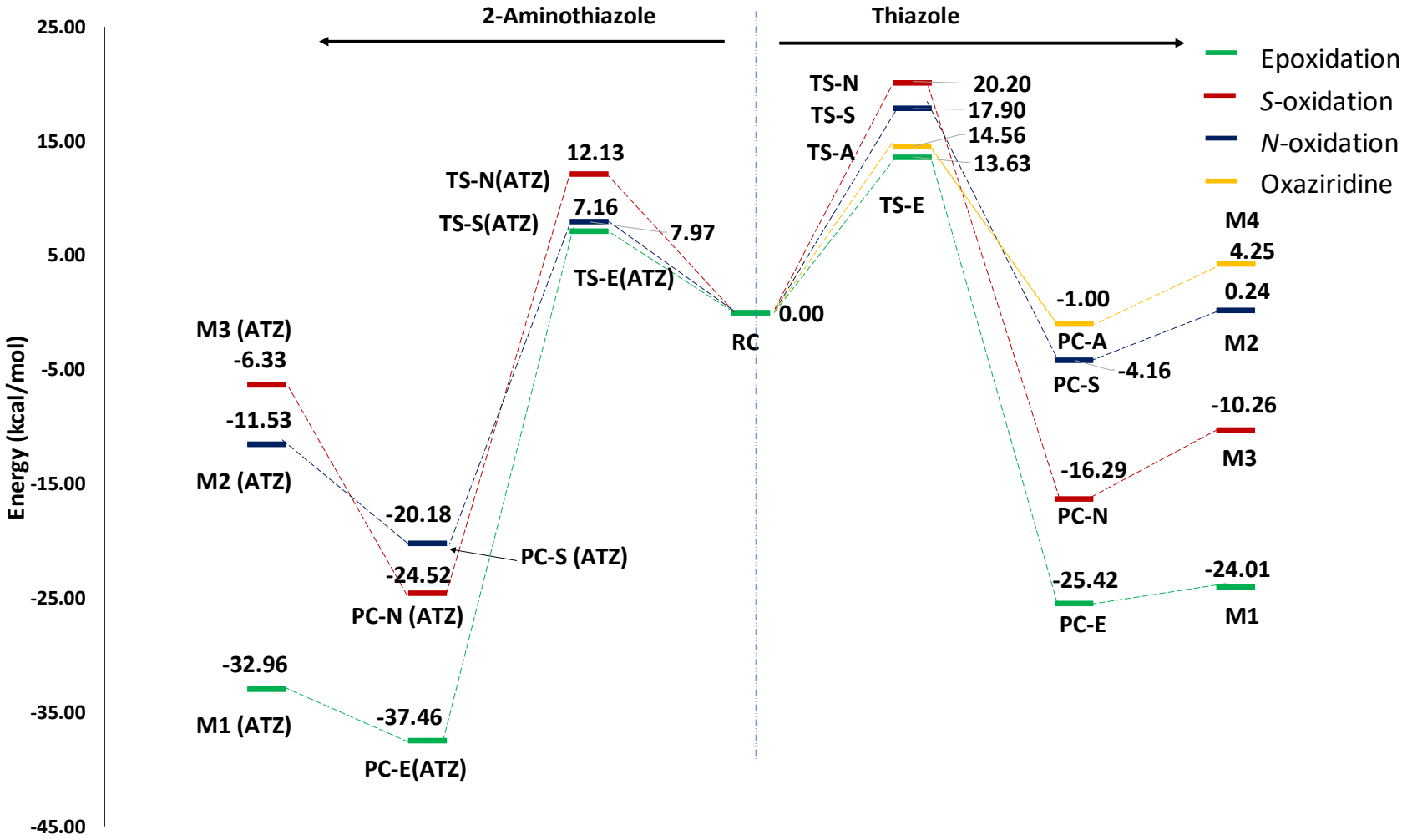


**Figure 5.** Energy profile comparison between TZ (right side) and ATZ (left side) (epoxidation, *S*-oxidation, *N*-oxidation, and oxaziridine formation in the presence of Cpd I) on the doublet potential energy surface of Cpd I. All the values are obtained using B3LYP(SCRF)/6-311++G(d,p)//B3LYP/6-31+G(d) basis set. Note that the release of the metabolite from the product complexes is an endergonic process in all cases.

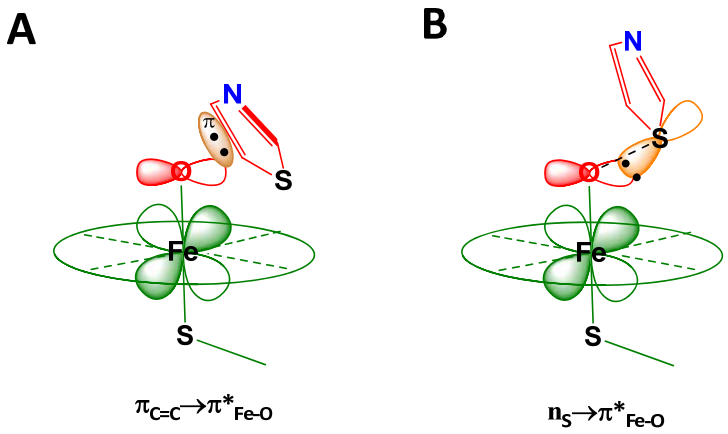


**Figure 6.** Participation of orbitals in the electron transfer during epoxidation and *S*-oxidation pathways (a) Cartoon representation of orbital overlap of the π-bond with the $\pi^*_{xz}$ orbital of heme in the doublet state (b) Cartoon representation of the orbital overlap of *S*-lone pair with $\pi^*_{xz}$ of heme in the doublet state.

***Oxaziridine formation*:** The formation of an oxaziridine metabolite is a rarely suggested pathway in drug metabolism. The oxaziridine reactive metabolite may be involved in apoprotein modification or covalent modification of DNA.[120–122] In the case of a 3-substituted indazole compound, the formation of oxaziridine was reported, mediated by several rat CYPs enzymes such as CYP3A1 and CYP3A2.[123–127] In contrast, the oxaziridine formation on TZ has not been reported. The barrier for the formation of an oxaziridine ring is 14.56 kcal/mol via a transition state **TS-A** (Figures 4, 5). The product complex (**PC-A**) is -1.00 kcal/mol more stable than the starting species, which is less favorable than the epoxidation product.

Figure 5 (right side) shows the PES for all the four reactions studied here, epoxidation, *S*-oxidation, *N*-oxidation, and oxaziridine formation in TZ. This comparison reveals that the epoxidation of **TZ** is thermodynamically and kinetically favorable compared to the *S*-oxidation, *N*-oxidation and oxaziridine formation reactions, although the barrier height for oxaziridine formation is only ~1 kcal/mol larger than for epoxidation, the oxaziridine metabolite (**M4**) is much less stable (by 13.75 kcal/mol) than **M1**. The PC complex of *N*-oxide product is as stable as epoxide product, but the barrier for its formation is ~ 7 kcal/mol higher. It can thus be concluded that the formation of epoxide on the TZ ring is the most favored CYP-mediated reaction.

*Influence of the amino group at $C^2$ in TZ*

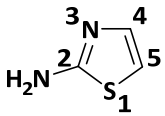


2-aminothiazole (ATZ)

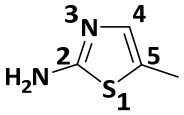


2-amino-5-methylthiazole (AMTZ)

**Figure 7.** Model compounds of 2-aminothiazole (**ATZ**) and 2-amino-5-methyl thiazole (**AMTZ**).

Metabolism studies on the oxidation of 2-aminothiazoles (e.g., sudoxicam) were extensively reported, during which the preferential formation of epoxidation products were observed.[11,12,26,29] In the current work, these reactions were modeled with the help of 2-aminothiazole (ATZ, Figure 7) and Cpd I. Figure 8 shows the optimized structures of the transition states on this reaction path. Figure 5 (left) provides the PES of the oxidation reactions of ATZ. In the case of ATZ also, the epoxidation reaction is the most preferred one, with a barrier of 7.16 kcal/mol in comparison to *S*-oxidation and *N*-oxidation reactions (7.97 and 12.13 kcal/mol respectively). The barrier for the epoxidation of ATZ is lower (7.16 kcal/mol) in comparison to the barrier for epoxidation of TZ (13.63 kcal/mol). This is well supported by the global nucleophilicity indices (*N*) -- for ATZ (1.01 eV) is higher than that of TZ (0.71 eV). The local nucleophilicity at the $C^5$ center of ATZ ($N$ = –0.60 eV) is slightly higher than that of $C^5$ centre of TZ ($N$ = –0.47 eV). The epoxide product complex involving ATZ is -37.46 kcal/mol more stable than the reactive complex. Similarly, *S*-oxidation and *N*-oxidation processes also become energetically more favorable in ATZ in comparison to TZ. For the oxaziridine formation from ATZ, it was not practical to identify a transition state (all attempts led to the *N*-oxidation path). The amine group at $C^2$- postion of ATZ can also undergoes *N*-hydroxylation, it is hypothesis that this mutagenicity originates from the reactive intermediate involving *N*-hydroxy metabolite. [128–130] To verify this hypothesis, quantum chemical study has been carried out, the barrier for the abstraction of a hydrogen radical from the $NH_2$ group is 7.53 kcal/mol, which leads to formation of a-radical intermediate, the radical intermediate forms *N*-hydroxy product via a rebound step (Figure S3). *N*-hydroxy metabolite can leads to mutagencity by interacting with DNA and proteins.These results are clearly indicating that it is possible to distinguish the preferred metabolic reaction of the thiazole containing compounds after successfully predicting the SOM. Table S3 provides a comparative analysis of the metabolites and isomers originating from TZ and ATZ. In the case of ATZ also the isomers are more stable than the metabolites. Also, the isomers **I10** and **I11** of ATZ metabolites are most electrophilic and most reactive with $MeO^-$. On a relative scale, the metabolites originating from ATZ are

marginally less electrophilic. Overall, it can be concluded that the metabolite formation becomes easier with 2-amino substitution, but the reactivity of the metabolites is not significantly altered due to 2-amino substitution.

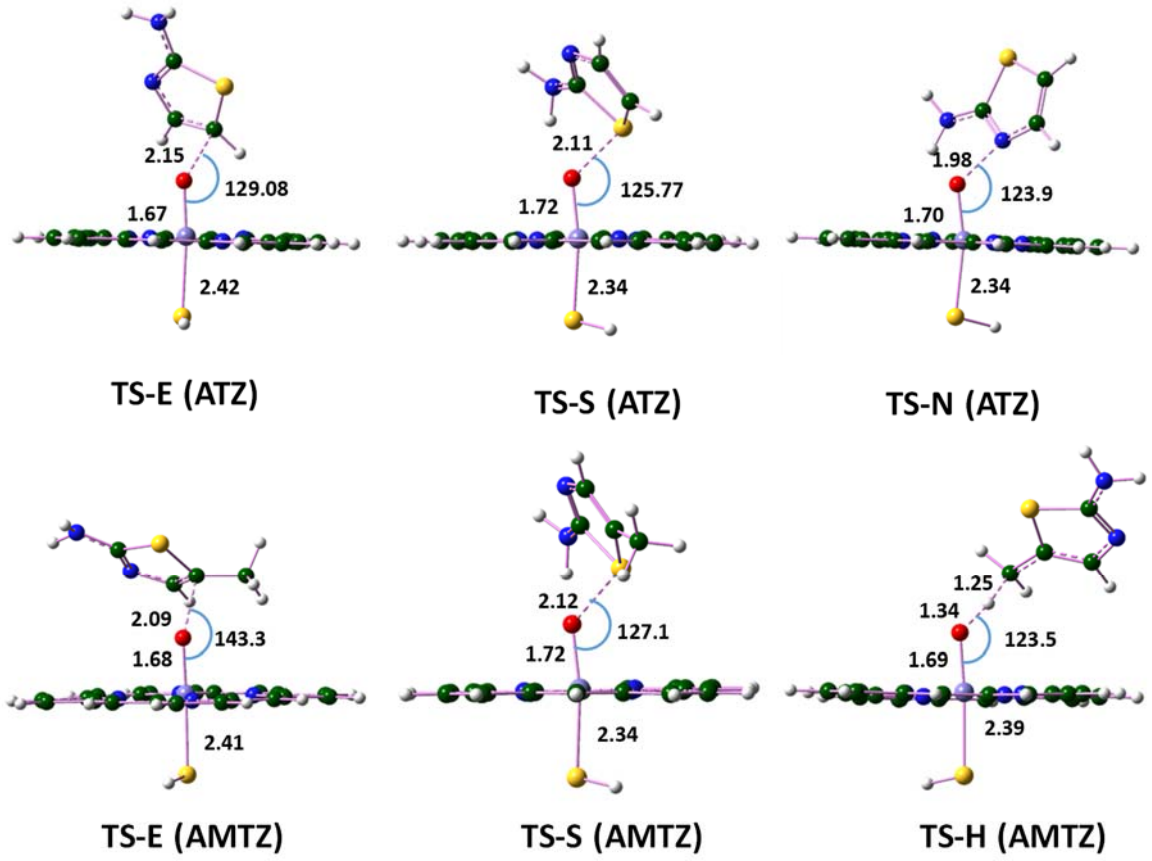


**Figure 8.** The transition states geometries of **TS-E, TS-S, TS-N** of ATZ and **TS-E, TS-S, TS-H** of AMTZ. All of the bond lengths are in Ångstrom (Å) and bond angles are in degrees (°).

***Influence of alkylation at $C^5$ position***

Toxicity studies on the drugs sudoxicam and meloxicam were extensively reported.[11,17,27,28] Although meloxicam only differs in the methyl group at $C^5$ position (Figure 1) from sudoxicam, clearly differential toxicity profiles were noticed.[17] To understand the biochemical changes in the metabolism of meloxicam, quantum chemical studies were performed on 2-amino-5-methyl-thiazole (AMTZ, Figure 7, 8) as a model compound and Cpd I. The energy barriers for the oxidation reactions are 16.63, 17.21, and 19.42 kcal/mol for epoxidation, *S*-oxidation, and *N*-oxidation, respectively in AMTZ (see ESI, Figure S4). The barrier for the abstraction of a hydrogen radical from the $C^5$-methyl group is 14.98 kcal/mol via **TS-H** (optimized structures of important transition states are provided in Figure 8). The hydroxy metabolite is highly stable (-45.50 kcal/mol) in comparison with epoxide, *S*-oxide, and *N*-oxide metabolites (-30.16, -13.03 and -16.01 kcal/mol, respectively) (see ESI, Figure S4). Moreover, the hydroxy product is non-toxic (although its oxidation products are toxic due to their electrophilicity). This indicates that the hydroxylation reaction is more preferred in the case of 2-amino-5-methyl-thiazole (meloxicam) than alternative oxidation reactions, which are favorable in the case of sudoxicam. This is well supported by the molecular docking results (Figure S6). In the first ranked pose of sudoxicam in the active site of the CYP2C9 and CYP3A4 isoforms, the $C^5$ atom of the thiazole ring is pointed towards the Fe=O center. At the same time, in the case of meloxicam the methyl group at $C^5$ is pointed towards the Fe=O center. Thus, in case of meloxicam hydroxylation at C5 -methyl of thiazole ring preferred, supporting the results from experimental observations (see ESI for docking poses, Figure S6).[131] Thus, the oxidation reactions that lead to the formation of toxic metabolites are avoided when an alkyl group is present at the $C^5$ position in TZ (or ATZ). Similarly, analysis has been carried out to identify the effect of alkylation at C4 position (C4-AMTZ), the results indicate that *S*-oxidation is more preferred in relation to other alternate pathways (see ESI, Figure S7).

**Reactions of epoxide reactive metabolite**

The epoxide metabolite (**M1**) of TZ is more stable than the *S*-oxide metabolite (**M2**), *N*-oxide metabolite (**M3**), and oxaziridine metabolite (**M4**) (Figures 4, 8) by 24.26, 13.75 and 36.75 kcal/mol respectively. All these primary metabolites are isomers; they can rearrange to other more stable isomers (**I5**-**I14**) (Figure 9). Although **M1** is not very electrophilic, many of its isomers are highly electrophilic (Table 3), undergo nucleophilic attacks (by amino acids and/or GSH) or undergo hydrolysis reactions. The isomers with high electrophilicity can be

toxic (Table 3). In the following sections, the relative energies of a few important isomers and their reactivity profiles are described.

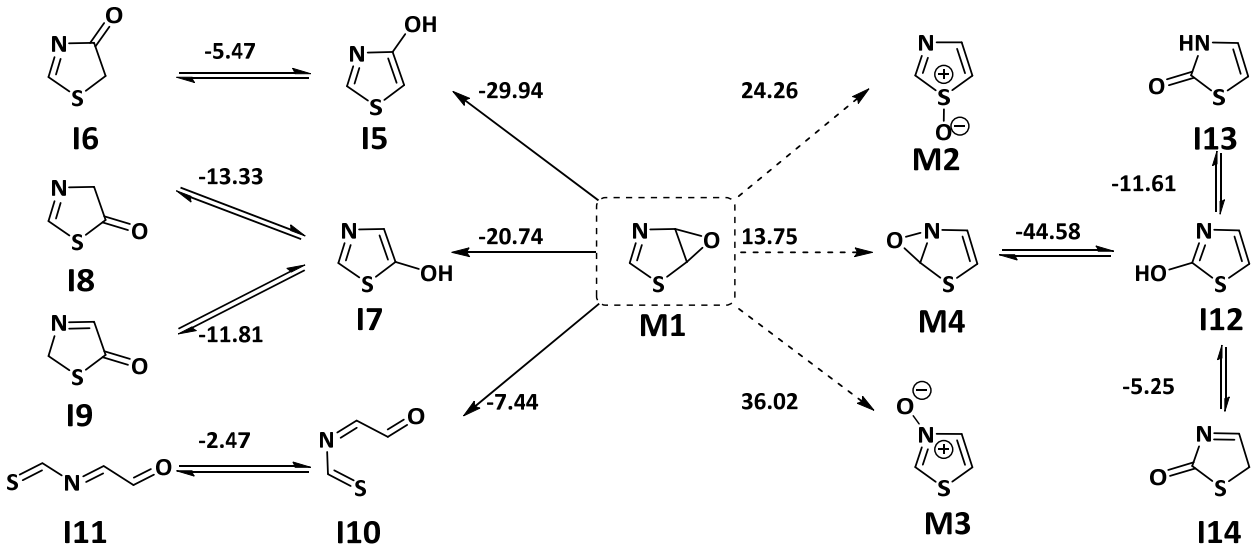


**Figure 9.** Isomers of the thiazole epoxide metabolite (**M1**). Arrows represent rearrangeable processes, dotted arrows represent only relative energy values (between non rearrangeable isomers). All of the energy values (in kcal/mol) on the arrow marks are ΔG values.

***Isomers***

**I5-I14** are structural isomers of **M1-M4**. Double oxidation is also possible on the thiazole rings,[5,9,18] many of these products have been reported to be toxic. It is important to establish the relative energies of all the isomers and double oxidation. The isomers **I5-I14** are more stable than **M1-M4** (Figure 9).

**M1** can undergo an acid-catalyzed 1,2-*H* shift, and the disruption of the epoxide ring by cleaving the $C^4$–O bond leads to the formation of isomer **I5**, a hydroxyl intermediate. Isomer **I5** can tautomerize to the 3-keto isomer **I6** via keto-enol tautomerism. The isomers **I5** and **I6** are more stable than **M1** (by 29.94 and 35.41 kcal/mol, respectively). The isomer **I7** is also a hydroxy isomer similar to **I5**, which can also be generated via an acid-catalyzed epoxide ring-opening process (breakage of $C^5$–O bond) from **I7**. The isomers **I8** and **I9** are the keto isomers of **M1** (via **I7**) through a 1,3-*H*-shift and a 1,5-*H*-shift (keto-enol tautomerism), respectively. Isomers **I7**–**I9** are also more stable than **M1**. The keto isomers (**I6**, **I8,** and **I9**) are more electrophilic than **M1**. The isomers **I8** and **I9** can undergo a hydrolysis reaction and lead to the formation of thiol products (after ring-opening), which can further react with cysteine (or GSH), leading to the formation of disulfide adducts. On the other hand, the double oxidation products **D1**–**D10** (Figure 10) are highly electrophilic and can lead to many toxic reactions with amino acids (especially when GSH levels are low).

The rearrangement of thiazole epoxide **M1** results in the generation of isomer **I10**, owing to the opening of both the five-membered and three-membered rings. This rearrangement is an exergonic process by 7.44 kcal/mol and with a barrier of 14.54 kcal/mol (**TS1**, Figure S8). The negative hyperconjugation originating from the bridging oxygen atom lone pairs of electrons of **M1** (breaking of S-$C^1$ bond) could be the driving force for this rearrangement. **I10** is highly electrophilic in nature with a high global electrophilicity index (ω = 4.26), which is much higher than that of **M1** (ω = 1.62). Nucleophilic residues or GSH can attack at $C^5$ position of **I10** and generate adducts. The isomer **I10** adopts a *cis* arrangement across the central imine unit, **I11** is the corresponding *trans* isomer, which is about 2.47 kcal/mol more stable than **I10**. **I11** is also highly electrophilic (ω = 4.38).

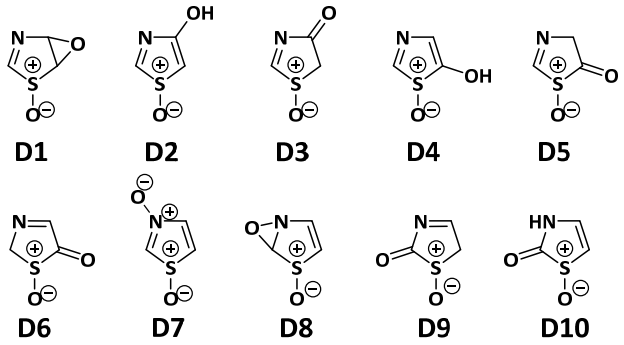


**Figure 10.** The 2D structures of possible double oxidation products (**D1 - D10**).

**Table 3.** The relative free energies (Δ*G*) and the global electrophilicity indices (ω) of the reactive metabolites. The activation energies ($E_a(MeO^-)$) for the reaction of the **RM** with $MeO^-$

| RMs | Relative Energy (Δ*G*)[a] | Electrophilicity (ω) | $E_a$ ($MeO^-$)[a] |
|---|---|---|---|
| **TZ** | - | 1.42 | - |
| **M1** | 0.00 | 1.62 | 9.54 |
| **M2** | 24.26 | 3.03 | 6.81 |
| **M3** | 13.75 | 1.62 | 18.41 |
| **M4** | 36.02 | 1.90 | 17.56 |
| **I5** | -29.94 | 1.37 | 21.75 |
| **I6** | -35.41 | 2.34 | 9.22 |
| **I7** | -20.74 | 1.37 | 21.01 |
| **I8** | -34.07 | 1.74 | 10.23 |
| **I9** | -32.55 | 2.57 | 9.14 |
| **I10** | -1.30 | 4.26 | 4.24 |
| **I11** | -9.91 | 4.38 | 4.01 |
| **I12** | -30.83 | 1.12 | 22.81 |
| **I13** | -42.45 | 0.99 | 23.45 |
| **I14** | -36.09 | 2.38 | 9.10 |
| **D1** | 54.91 | 4.87 | 3.95 |
| **D2** | 18.77 | 3.00 | 7.58 |
| **D3** | 2.63 | 3.26 | 8.14 |
| **D4** | 26.24 | 2.81 | 10.75 |
| **D5** | 12.14 | 2.69 | 8.74 |
| **D6** | 9.82 | 4.04 | 6.71 |
| **D7** | 59.41 | 3.35 | 6.53 |
| **D8** | 68.01 | 2.68 | 11.45 |
| **D9** | 2.75 | 3.27 | 6.42 |
| **D10** | 0.00 | 2.19 | 9.15 |

[a]In kcal/mol.

***Nucleophilic attack***

In the active site of CYPs, a few nucleophilic amino acid residues are present, which are suggested to be responsible for the opening of the epoxide ring and the formation of a covalent adduct, leading to the inhibition of CYPs by MBI. For this purpose, the crystal structures of various isoforms of cytochrome (CYP 3A4, 2C9, 2C19 and 2D6; downloaded from the Protein Data Dank) were analyzed. Various nucleophilic amino acids (serine, threonine, cysteine, arginine, and lysine) were identified in the vicinity of the heme-porphyrins (within 5 Å distance) (Table S2). For example, threonine is present in the active site of most CYP isoforms, it participates in the proton relay mechanism from a carboxylate side chain to the distal oxygen of Compound 0 (ferric-hydroperoxo species) resulting in the formation of the active species Cpd I.[132] The nucleophilic residues are active at the ROH or RSH group. The oxygen/sulfur atom lone pair of electrons attack the electrophilic **M2**. Alternatively, the OH/SH group can also first be get ionized to $RO^{-}$/$RS^{-}$ with the help of basic residues and react.

In our previous studies, it was realized that Ser/Thr react in an anionic rather than neutral state under physiological conditions.[31,32,34] Thus, the nucleophilic addition reactions were studied only with anionic species $MeO^{-}$ and $MeS^{-}$ (as models of anionic serine and cysteine). Figure 11 shows the nucleophilic addition reactions of **M1** by the model nucleophiles. The energy barrier for the nucleophilic attack reaction between **M1** and $MeO^{-}$ is 9.54 kcal/mol (**TS2**, Figure S8). Likewise, the energy barrier for the reaction between **M1** and $MeS^{-}$ is 15.98 kcal/mol (**TS3**, Figure S8). Thus, the barriers for nucleophilic attack by Ser/Thr/Cys are small, so Ser/Thr/Cys can cause MBI via the acid−base enzyme catalysis processes, which generate their adducts due to nucleophilic attack.

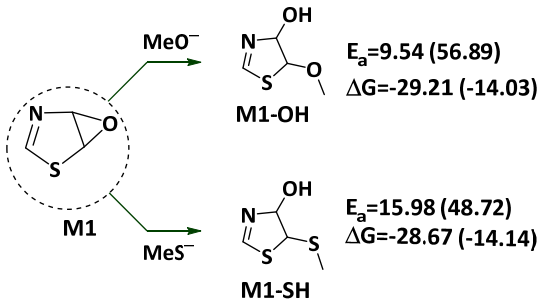


**Figure 11.** Nucleophilic addition reactions of the isomer **M1**. All of the energy values are in kcal/mol. The values given are for the reactions of **M1** with anionic (neutral) species.

***Hydrolysis***

The epoxide metabolite **M1** can also undergo a hydrolysis reaction by water molecule(s) directly in the cavity of the enzyme. The final metabolites **M5** and **M6** originating from this hydrolysis process have been suggested from experimental studies,[152,153] this can be explained as shown in Figure 12. Hydrolysis of **M1** initially results in the generation of the vicinal diol **M1-D**, which is generally non-toxic. In the hydrolysis reaction, a water molecule attacks at the $C^4/C^5$ centers of **M1**. The predicted electrophilicity is larger at $C^5$ than at $C^4$, thus, it is more likely that the attack of $H_2O$ happens at the $C^5$ center. The formation of **M1-D** is an exergonic process by -12.85 kcal/mol, requiring an energy barrier of 28.45 kcal/mol via **TS4** (Figure 12). The vicinal diol can undergo ring-chain tautomerism[133] to generate α-hydroxy aldehyde intermediates: a 1,3-*H*-shift from the 4-hydroxy group leads to the generation of **HM1** (by breaking the $N–C^4$ bond) and a 1,5-*H*-shift from the 5-hydroxy group leads to the formation of **HM2** (by breaking the $S–C^5$ bond). The *H*-shift reaction can occur directly (unimolecular process) or be assisted by a water molecule (bimolecular process). The formation of **HM1** from **M1-D** requires barriers of 25.17 kcal/mol via **TS5′** (43.44 kcal/mol without the assistance of a water molecule via **TS5**, Figure 13). Similarly, the formation of **HM2** from **M1-D** requires a barrier of 24.82 kcal/mol via **TS7′** (37.85 kcal/mol without the assistance of a water molecule via **TS7**). **HM1** and **HM2** can undergo one more *H*-shift process leading to the generation of the experimentally reported metabolites **M5** and **M6** by breaking $S–C^5$ and $N–C^4$ bonds, respectively, for which the estimated barriers are 4.26 kcal/mol and 3.95 kcal/mol, respectively. The formation of such metabolites were implicated in toxicity.[134,135]

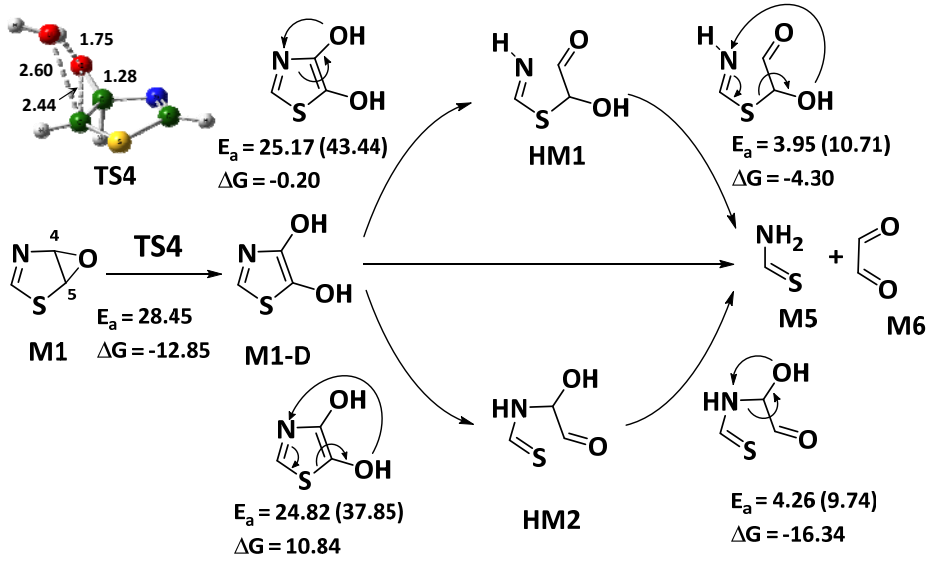


**Figure 12.** Hydrolysis of the epoxide metabolite **M1** with the assistance of water. The values in parenthesis are in the absence of water mediation. All of the energy values are in kcal/mol.

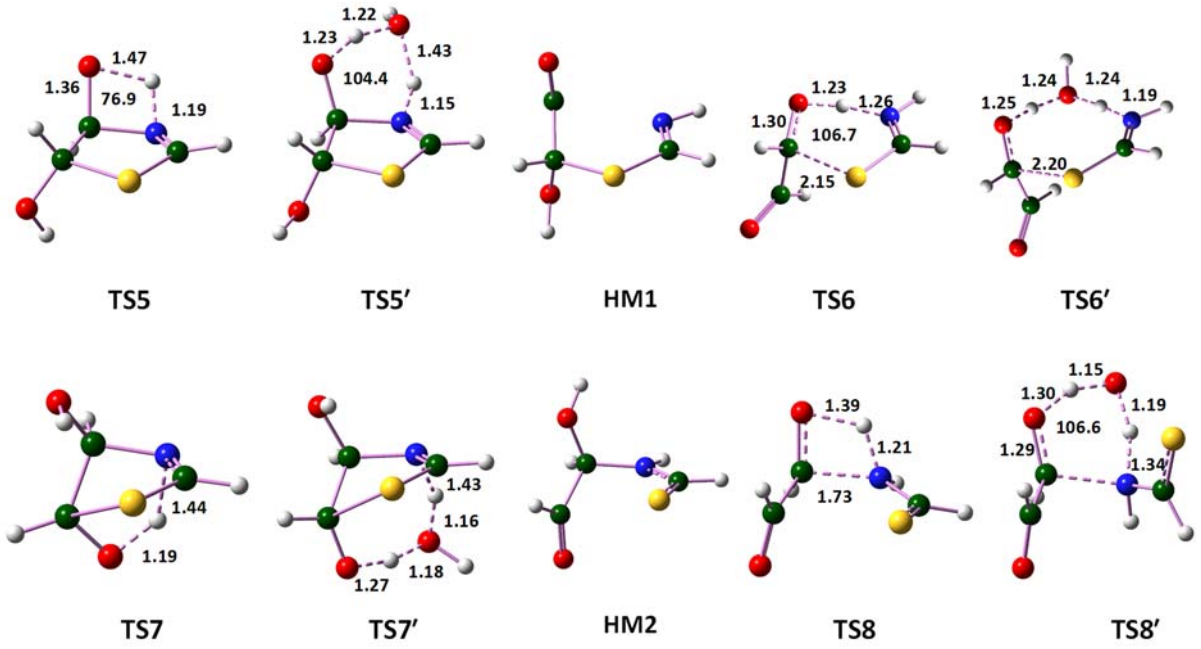


**Figure 13**. The optimized structures of the intermediates and transition states involved in the hydrolysis of epoxide metabolite (Figure 12). All of the distances are in angstroms (Å) and angles are in degree (°).

It can be expected that not only **M1-M4**, but also all of the other possible isomers and dioxidation products, can react with nucleophilic amino acids, especially because some of the alternative isomers are more electrophilic than **M1-M4**. Thus, it can be envisaged that the toxic effects may be originating from such isomeric metabolites. The reactions of all of these metabolites (**M1-M4**, **I5-I14**, **D1–D10**) were carried out with $MeO^-$ (a model of anionic serine). Table 3 shows the activation energy values for reactions of the isomers with $MeO^-$. These values suggest that the greater the electrophilicity of the isomer, the lower is the energy barrier for the reaction with $MeO^-$. For example, isomer **I11** requires a very low barrier (4.01 kcal/mol) for the reaction with $MeO^-$ in comparison to **M1** (9.54 kcal/mol). Similarly, in the case of dioxidation metabolite isomers, there are a few isomers such as **D1** that require a small activation energy (3.95 kcal/mol). The above analysis establishes that a few of the metabolites can produce covalent adducts with nucleophilic amino acids, leading to the inactivation of CYPs via MBI. Isomers that should be kept in watch list in that respect are **M2**, **I10**, **I11**, **D1**, **D2**, **D3**, **D6**, **D7** and **D9**, all of which are characterized by a global electrophilicity > 3 units. Hence, it is advisable to design thiazole derivatives such that the formation of such RMs is avoided.

## Conclusions

Molecular docking analysis has been carried out to explore preferred site of metabolism of thiazole containing drugs, the results are partially successful. The pathways associated with the biotransformation of thiazole ring-containing drugs mediated by CYPs have been explored using quantum chemical methods. The DFT (B3LYP(SCRF)/6-311++G(d,p)//B3LYP/6-31+G(d)) studies were employed to investigate the mechanistic details associated with four important biotransformation pathways (epoxidation, *S*-oxidation, *N*-oxidation, and oxaziridine formation) of the model compounds thiazole (TZ) and 2-aminothiazole (ATZ). The epoxidation process involves an initial attack of the $C^5$ carbon of the thiazole ring at the Fe=O oxygen center, which requires an energy barrier of 13.63 kcal/mol and is exergonic by 24.01 kcal/mol. The alternative reactions require either higher barriers or lead to less stable products. The epoxidation reaction becomes more favorable due to the presence of an amine group at the $C^2$ position, but the same reaction becomes less favorable when $C^5$ position is blocked (e.g., a methyl group at the $C^5$ position).

The four RMs (**M1**-**M4**) of thiazoles can rearrange to additional ten more isomers via simple chemical rearrangements. The global electrophilicity values of these fourteen reactive species were estimated. The electrophilicity of the initial metabolites is not very high, however, their isomers may be highly electrophilic and thus toxic (Ex. **I10** and **I11**). The metabolites (or their isomers) can directly form covalent adducts due to nucleophilic addition reaction with threonine/serine. The barrier for the reaction between the epoxide RM and $MeO^-$ (a model of anionic serine/threonine) was found to be small (~10 kcal/mol). These type of reactions possibly lead to MBI complex formation. The energy profile of the hydrolysis pathways from the epoxide metabolites leading to the formation of a protoxin was also explored. Overall, this study provided the atomic-level details of the metabolic processes associated with thiazole containing drugs and helped in identifying the toxic versus non-toxic reactive metabolites.

## Supporting Information

The supporting information is available free of charge on the ACS Publication website at DOI:10.1021/acs.chemrestox.XXXXX

The complete details of Cartesian coordinates of all the structures considered in this study, estimated Gibbs free energy values of all the species considered in the reactions, electrophilicity indices of 2-amino thiazole, Gibbs free energy profiles of catalytic cycles of 2-amino-5-methyl thiazole and 2-amino-4-methyl thiazole are provided.

### Abbreviations

AMTZ, 2-amino-5-methylthiazole; ATZ, Aminothiazole; B3LYP, Becke 3 Lee-Yang-Parr; Cpd I, Compound I (Model of heme porphine catalytic domain of CYP); CYPs, Cytochromes; DFT, Density Functional Theory; DOT, Direct Oxygen Transfer; GSH, Glutathione; HOMO, Highest Occupied Molecular Orbital; I-E, Intermediate radical complex; IEFPCM, Integral Equation Formalism variant of the Polarizable Continuum Model; LANL2DZ, Los Alamos National Laboratory 2 Double Zeta; LC–MS, Liquid Chromatography-Mass Spectroscopy; LUMO, Lowest Unoccupied Molecular Orbital; MBI, Mechanism-Based Inhibition/Inactivation; MICs, Metabolic Intermediate Complexes; MO, Molecular Orbital; PC, Product Complex; PES, Potential Energy Surface; QC, Quantum Chemical; RC, Reaction Complex; RMs, Reactive Metabolites; SARS-CoV2, Severe Acute Respiratory Syndrome-Coronavirus2; SCRF, Self-Consistent Reaction Field; TS, Transition State; TZ, Thiazole.

## Acknowledgments

This study was funded by the BundesministeriumfürBildung und Forschung (BMBF), Germany, within the project “ReMetaDrug” (grant no. 01DQ19002 to HG). HG is grateful for computational support by the “ZentrumfürInformations- und Medientechnologie” at the Heinrich-Heine-Universität Düsseldorf and the computing time provided by the John von Neumann Institute for Computing (NIC) to HG on the supercomputer JUWELS at Jülich Supercomputing Centre (JSC) (user IDs: HKF7). PVB thanks the Department of Biotechnology (DBT), New Delhi for the same joint project between India and Germany in the field of Health Informatics, Project No- BT/IN/BMBF-BioHR/30/PVB/2018-2019.

## References


(1) Kalgutkar, A. S.; Didiuk, M. T. Structural Alerts, Reactive Metabolites, and Protein Covalent Binding: How Reliable Are These Attributes as Predictors of Drug Toxicity? *Chem. Biodivers.* **2009**, *6* (11), 2115–2137. https://doi.org/10.1002/cbdv.200900055.

(2) Kalgutkar, A. S.; Fate, G.; Didiuk, M. T.; Bauman, J. Toxicophores, Reactive Metabolites and Drug Safety: When Is It a Cause for Concern? *Expert Rev. Clin. Pharmacol.* **2008**, *1* (4), 515–531. https://doi.org/10.1586/17512433.1.4.515.

(3) Kalgutkar, A. S.; R. Scott Obach; Tristan S. Maurer. Mechanism-Based Inactivation of Cytochrome P450 Enzymes: Chemical Mechanisms, Structure-Activity Relationships and Relationship to Clinical Drug-Drug Interactions and Idiosyncratic Adverse Drug Reactions. *Curr. Drug Metab.* **2007**, *8* (5), 407–447. https://doi.org/10.2174/138920007780866807.

(4) Stachulski, A. V; Baillie, T. A.; Park, B. K.; Obach, R. S.; Dalvie, D. K.; Williams, D. P.; Srivastava, A.; Regan, S. L.; Antoine, D. J.; Goldring, C. E. P.; Chia, A. J. L.; Kitteringham, N. R.; Randle, L. E.; Callan, H.; Castrejon, J. L.; Farrell, J.; Naisbitt, D. J.; Lennard, M. S. The Generation, Detection, and Effects of Reactive Drug Metabolites. *Med. Res. Rev.* **2012**, *33* (5), 1–96. https://doi.org/10.1002/med.

(5) Stepan, A. F.; Walker, D. P.; Bauman, J.; Price, D. A.; Baillie, T. A.; Kalgutkar, A. S.; Aleo, M. D. Structural Alert/Reactive Metabolite Concept as Applied in Medicinal Chemistry to Mitigate the Risk of Idiosyncratic Drug Toxicity: A Perspective Based on the Critical Examination of Trends in the Top 200 Drugs Marketed in the United States. *Chem. Res. Toxicol.* **2011**, *24* (9), 1345–1410. https://doi.org/10.1021/tx200168d.

(6) Hewitt, M.; Enoch, S. J.; Madden, J. C.; Przybylak, K. R.; Cronin, M. T. D. Hepatotoxicity: A Scheme for Generating Chemical Categories for Read-across, Structural Alerts and Insights into Mechanism(s) of Action. *Crit. Rev. Toxicol.* **2013**, *43* (7), 537–558. https://doi.org/10.3109/10408444.2013.811215.

(7) Walsh, J. S.; Miwa, G. T. Bioactivation of Drugs: Risk and Drug Design. *Annu. Rev. Pharmacol. Toxicol.* **2011**, *51* (1), 145–167. https://doi.org/10.1146/annurev-pharmtox-010510-100514.

(8) Sushko, I.; Salmina, E.; Potemkin, V. A.; Poda, G.; Tetko, I. V. ToxAlerts: A Web Server of Structural Alerts for Toxic Chemicals and Compounds with Potential Adverse Reactions. *J. Chem. Inf. Model.* **2012**, *52* (8), 2310–2316. https://doi.org/10.1021/ci300245q.

(9) Dalvie, D. K.; Kalgutkar, A. S.; Khojasteh-Bakht, S. C.; Obach, R. S.; O'Donnell, J. P.; O'Donnell, J. P. Biotransformation Reactions of Five-Membered Aromatic Heterocyclic Rings. *Chem. Res. Toxicol.* **2002**, *15* (3), 269–299. https://doi.org/10.1021/tx015574b.

(10) Gramec, D.; Peterlin Mašič, L.; Sollner Dolenc, M. Bioactivation Potential of Thiophene-Containing Drugs. *Chem. Res. Toxicol.* **2014**, *27* (8), 1344–1358. https://doi.org/10.1021/tx500134g.

(11) Kalgutkar, A. S. Tracking Where the O's Go. *ACS Cent. Sci.* **2015**, *1* (4), 163–165. https://doi.org/10.1021/acscentsci.5b00231.

(12) Kalgutkar, A. S.; Dalvie, D. Predicting Toxicities of Reactive Metabolite–Positive Drug Candidates. *Annu. Rev. Pharmacol. Toxicol.* **2015**, *55* (1), 35–54. https://doi.org/10.1146/annurev-pharmtox-010814-124720.

(13) Siddiqui, N.; Arshad, M. F.; Ahsan, W.; Alam, M. S. Thiazoles : A Valuable Insight into the Recent Advances and Biological Activities. *Ijpsdr* **2009**, *1* (3), 136–143.

(14) Das, D.; Sikdar, P.; Bairagi, M. Recent Developments of 2-Aminothiazoles in Medicinal Chemistry. *Eur. J. Med. Chem.* **2016**, *109*, 89–98. https://doi.org/10.1016/j.ejmech.2015.12.022.

(15) Jeong, H. J.; Min, S.; Chae, H.; Kim, S.; Lee, G.; Namgoong, S. K.; Jeong, K. Signal Amplification by Reversible Exchange for COVID-19 Antiviral Drug Candidates. *Sci. Rep.* **2020**, *10* (1), 14290. https://doi.org/10.1038/s41598-020-71282-6.

(16) Serafin, M. B.; Bottega, A.; Foletto, V. S.; da Rosa, T. F.; Hörner, A.; Hörner, R. Drug Repositioning Is an Alternative for the Treatment of Coronavirus COVID-19. *Int. J. Antimicrob. Agents* **2020**, *55* (6), 105969. https://doi.org/10.1016/j.ijantimicag.2020.105969.

(17) Obach, R. S.; Kalgutkar, A. S.; Ryder, T. F.; Walker, G. S. In Vitro Metabolism and Covalent Binding of Enol-Carboxamide Derivatives and Anti-Inflammatory Agents Sudoxicam and Meloxicam: Insights into the Hepatotoxicity of Sudoxicam. *Chem. Res. Toxicol.* **2008**, *21* (9), 1890–1899. https://doi.org/10.1021/tx800185b.

(18) Orr, S. T. M.; Ripp, S. L.; Ballard, T. E.; Henderson, J. L.; Scott, D. O.; Obach, R. S.; Sun, H.; Kalgutkar, A. S. Mechanism-Based Inactivation (MBI) of Cytochrome P450 Enzymes: Structure-Activity Relationships and Discovery Strategies to Mitigate Drug-Drug Interaction Risks. *J. Med. Chem.* **2012**, *55* (11), 4896–4933. https://doi.org/10.1021/jm300065h.

(19) Mizutani, T.; Yoshida, K.; Kawazoe, S. Formation of Toxic From and Other Thiazole n Mice Identification of Thioamides as Ring Cleavage of Products. *Drug Metab. Dispos.* **1994**, *22* (5), 750–755.

(20) Mizutani, T.; Suzuki, K. Relative Hepatotoxicity of 2-(Substituted Phenyl)Thiazoles and Substituted Thiobenzamides in Mice: Evidence for the Involvement of Thiobenzamides as Ring Cleavage Metabolites in the Hepatotoxicity of 2-Phenylthiazoles. *Toxicol. Lett.* **1996**, *85* (2), 101–105. https://doi.org/10.1016/0378-4274(96)03646-6.

(21) Mizutani, T.; Yoshida, K.; Kawazoe, S. Possible Role of Thioformamide as a Proximate Toxicant in the Nephrotoxicity of Thiabendazole and Related Thiazoles in Glutathione-Depleted Mice: Structure-Toxicity and Metabolic Studies. *Chem. Res. Toxicol.* **1993**, *6* (12), 174–179.

(22) Kalgutkar, A. S.; Driscoll, J.; Zhao, S. X.; Walker, G. S.; Shepard, R. M.; Soglia, J. R.; Atherton, J.; Yu, L.; Mutlib, A. E.; Munchhof, M. J.; Reiter, L. A.; Jones, C. S.; Doty, J. L.; Trevena, K. A.; Shaffer, C. L.; Ripp, S. L. A Rational Chemical Intervention Strategy to Circumvent Bioactivation Liabilities Associated with a Nonpeptidyl Thrombopoietin Receptor Agonist Containing a 2-Amino-4-Arylthiazole Motif. *Chem. Res. Toxicol.* **2007**, *20* (12), 1954–1965. https://doi.org/10.1021/tx700270r.

(23) Lakshmi, V. M.; Zenser, T. V; Sohani, S.; Davis, B. B. Mechanism of Formation of the Thioether Conjugate of the Bladder Carcinogen 2-Amino-4-(5-Nitro-2-Furyl)-Thiazole (ANFT). *Carcinogenesis* **1992**, *13* (11), 2087–2093.

(24) Lakshmi, V. M.; Mattammal, M. B.; Zenser, T. V; Davis, B. B. Mechanism of Peroxidative Activation of the Bladder Carcinogen 2-Amino-4-(5-Nitro-2-Furyl)-Thiazole (ANFT): Comparison with Benzidine. *Carcinogenesis* **1990**, *11* (11), 1965–1970.

(25) Offen, C. P.; Frearson, M. J.; Wilson, K.; Burnett, D. 4,5-Dimethylthiazole- *N* -Oxide- *S* -Oxide: A Metabolite of Chlormethiazole in Man. *Xenobiotica* **1985**, *15* (6), 503–511. https://doi.org/10.3109/00498258509045024.

(26) Subramanian, R.; Lee, M. R.; Allen, J. G.; Bourbeau, M. P.; Fotsch, C.; Hong, F. T.; Tadesse, S.; Yao, G.; Yuan, C. C.; Surapaneni, S.; Skiles, G. L.; Wang, X.; Wohlhieter, G. E.; Zeng, Q.; Zhou, Y.; Zhu, X.; Li, C. Cytochrome P450-Mediated Epoxidation of 2-Aminothiazole-Based AKT Inhibitors: Identification of Novel GSH Adducts and Reduction of Metabolic Activation through Structural Changes Guided by in Silico and in Vitro Screening. *Chem. Res. Toxicol.* **2010**, *23* (3), 653–663. https://doi.org/10.1021/tx900414g.

(27) Leung, L.; Kalgutkar, A. S.; Obach, R. S. Metabolic Activation in Drug-Induced Liver Injury. *Drug Metab. Rev.* **2012**, *44* (1), 18–33. https://doi.org/10.3109/03602532.2011.605791.

(28) Zuniga, F. I.; Loi, D.; Ling, K. H. J.; Tang-Liu, D. D. Idiosyncratic Reactions and Metabolism of Sulfur-Containing Drugs. *Expert Opin. Drug Metab. Toxicol.* **2012**, *8* (4), 467–485. https://doi.org/10.1517/17425255.2012.668528.

(29) Hobbs, D. C.; Twomey, T. M. Metabolism of Sudoxicam by the Rat, Dog, and Monkey. *Drug Metab. Dispos.* **1977**, *5* (1), 75–81.

(30) Taxak, N.; Desai, P. V; Patel, B.; Mohutsky, M.; Klimkowski, V. J.; Gombar, V.; Bharatam, P. V. Metabolic-Intermediate Complex Formation with Cytochrome P450: Theoretical Studies in Elucidating the Reaction Pathway for the Generation of Reactive Nitroso Intermediate. *J. Comput. Chem.* **2012**, *33* (21), 1740–1747. https://doi.org/10.1002/jcc.23008.

(31) Taxak, N.; Kalra, S.; Bharatam, P. V. Mechanism-Based Inactivation of Cytochromes by Furan Epoxide: Unraveling the Molecular Mechanism. *Inorg. Chem.* **2013**, *52* (23), 13496–13508. https://doi.org/10.1021/ic401907k.

(32) Taxak, N.; Dixit, V. A.; Bharatam, P. V. Density Functional Study on the Cytochrome-Mediated S-Oxidation: Identification of Crucial Reactive Intermediate on the Metabolic Path of Thiazolidinediones. *J. Phys. Chem. A* **2012**, *116* (42), 10441–10450. https://doi.org/10.1021/jp308023g.

(33) Taxak, N.; Parmar, V.; Patel, D. S.; Kotasthane, A.; Bharatam, P. V. S-Oxidation of Thiazolidinedione with Hydrogen Peroxide, Peroxynitrous Acid, and C4a-Hydroperoxyflavin: A Theoretical Study. *J. Phys. Chem. A* **2011**, *115* (5), 891–898. https://doi.org/10.1021/jp109935k.

(34) Jaladanki, C. K.; Taxak, N.; Varikoti, R. A.; Bharatam, P. V. Toxicity Originating from Thiophene Containing Drugs: Exploring the Mechanism Using Quantum Chemical Methods. *Chem. Res. Toxicol.* **2015**, *28* (12), 2364–2376. https://doi.org/10.1021/acs.chemrestox.5b00364.

(35) Taxak, N.; Patel, B.; Bharatam, P. V. Carbene Generation by Cytochromes and Electronic Structure of Heme-Iron-Porphyrin-Carbene Complex: A Quantum Chemical Study. *Inorg. Chem.* **2013**, *52* (9), 5097–5109. https://doi.org/10.1021/ic400010d.

(36) DrugBank: https://go.drugbank.com/.

(37) LigPrep, Schrödinger, LLC, New York, NY, 2018. LigPrep, Version 2.5, Schrödinger, LLC. **2012**.

(38) Harder, E.; Damm, W.; Maple, J.; Wu, C.; Reboul, M.; Xiang, J. Y.; Wang, L.; Lupyan, D.; Dahlgren,

M. K.; Knight, J. L.; Kaus, J. W.; Cerutti, D. S.; Krilov, G.; Jorgensen, W. L.; Abel, R.; Friesner, R. A. OPLS3: A Force Field Providing Broad Coverage of Drug-like Small Molecules and Proteins. *J. Chem. Theory Comput.* **2016**, *12* (1), 281–296. https://doi.org/10.1021/acs.jctc.5b00864.

(39) Protein Preparation Wizard, Schrödinger Suite 2018-4, LLC, NewYork, NY, 2018. Protein Preparation Wizard, Schrödinger Suite 2018-4, LLC, NewYork, NY, 2018.

(40) Glide, Schrödinger, LLC, New York, NY, 2018. Glide, Schrödinger, LLC, New York, NY, 2018.

(41) Frisch, M. J., Trucks, G. W., Schlegel, H. B., Scuseria, G. E.; Robb, M. A., Cheeseman, J. R., Scalmani, G., Barone, V., Mennucci, B.; Petersson, G. A., Nakatsuji, H., Caricato, M., Li, X., Hratchian, H. P.; Izmaylov, A. F., Bloino, J., Zheng, G., Sonnenberg, J. L., Hada, M.; Ehara, M., Toyota, K., Fukuda, R., Hasegawa, J., Ishida, M. . N.; T., Honda, Y., Kitao, O., Nakai, H., Vreven, T., Montgomery, J. A., J.; Peralta, J. E., Ogliaro, F., Bearpark, M., Heyd, J. J., Brothers, E., K.; K. N., Staroverov, V. N., Keith, T., Kobayashi, R., Normand, J.; Raghavachari, K., Rendell, A., Burant, J. C., Iyengar, S. S., Tomasi, J.; Cossi, M., Rega, N., Millam, J. M., Klene, M., Knox, J. E., Cross, J. B.; Bakken, V., Adamo, C., Jaramillo, J., Gomperts, R., Stratmann, R. E.; Yazyev, O., Austin, A. J., Cammi, R., Pomelli, C., Ochterski, J. W.; Martin, R. L., Morokuma, K., Zakrzewski, V. G., Voth, G. A., S.; P., Dannenberg, J. J., Dapprich, S., Daniels, A. D., Farkas, O.; Foresman, J. B., Ortiz, J. V., Cioslowski, J., and Fox, D. J. Gaussian 09. *Gaussian 09*. Gaussian, Inc.: Wallingford CT 2010.

(42) Shaik, S.; Cohen, S.; Wang, Y.; Chen, H.; Kumar, D.; Thiel, W. P450 Enzymes: Their Structure, Reactivity, and Selectivity-Modeled by QM/MM Calculations. *Chem. Rev.* **2010**, *110* (2), 949–1017. https://doi.org/10.1021/cr900121s.

(43) Meunier, B.; de Visser, S. P.; Shaik, S. Mechanism of Oxidation Reactions Catalyzed by Cytochrome P450 Enzymes. *Chem. Rev.* **2004**, *104* (9), 3947–3980. https://doi.org/10.1021/cr020443g.

(44) Himo, F.; Siegbahn, P. E. M. Quantum Chemical Studies of Radical-Containing Enzymes. *Chem. Rev.* **2003**, *103* (6), 2421–2456. https://doi.org/10.1021/cr020436s.

(45) Hirao, H.; Thellamurege, N.; Zhang, X. Applications of Density Functional Theory to Iron-Containing Molecules of Bioinorganic Interest. *Front. Chem.* **2014**, *2*, 14. https://doi.org/10.3389/fchem.2014.00014.

(46) Rydberg, P.; Olsen, L.; Ryde, U. Quantum-Mechanical Studies of Reactions Performed by Cytochrome P450 Enzymes. *Curr. Inorg. Chem.* **2012**, *2* (3), 292–315. https://doi.org/10.2174/1877944111202030292.

(47) Jaladanki, C. K.; Gahlawat, A.; Rathod, G.; Sandhu, H.; Jahan, K.; Bharatam, P. V. Mechanistic Studies on the Drug Metabolism and Toxicity Originating from Cytochromes P450. *Drug Metab. Rev.* **2020**, *52* (3), 366–394. https://doi.org/10.1080/03602532.2020.1765792.

(48) Parr, R.G.; Yang, W. E. Density Functional Theory of Atoms and Molecules; Oxford University Press: New York, 1989; pp 1–325.

(49) Becke, A. D. Density Functional Exchange Energy Approximation with Correct Asymptotic Behavior. *Phys. Rev. A* **1988**, *38* (6), 3098–3100.

(50) Krishnan, R.; Binkley, J. S.; Seeger, R.; Pople, J. A. Self Consistent Molecular Orbital Methods. XX. A

Basis Set for Correlated Wave Functions. *J. Chem. Phys.* **1980**, *72* (1), 650–654. https://doi.org/10.1063/1.438955.

(51) Hehre, W. J.; Ditchfield, R.; Pople, J. A. Self—Consistent Molecular Orbital Methods. XII. Further Extensions of Gaussian—Type Basis Sets for Use in Molecular Orbital Studies of Organic Molecules. *J. Chem. Phys.* **1972**, *56* (5), 2257–2261. https://doi.org/10.1063/1.1677527.

(52) Hehre, W. J. Ab Initio Molecular Orbital Theory. *Acc. Chem. Res.* **1976**, *9* (11), 399–406. https://doi.org/10.1021/ar50107a003.

(53) Hay, P. J.; Wadt, W. R. Ab Initio Effective Core Potentials for Molecular Calculations. Potentials for the Transition Metal Atoms Sc to Hg. *J. Chem. Phys.* **1985**, *82* (1), 270–283. https://doi.org/10.1063/1.448799.

(54) Tomasi, J.; Mennucci, B.; Cammi, R. Quantum Mechanical Continuum Solvation Models. *Chem. Rev.* **2005**, *105* (8), 2999–3093. https://doi.org/10.1021/cr9904009.

(55) Chattaraj, P. K.; Sarkar, U.; Roy, D. R. Electrophilicity Index. *Chem. Rev.* **2006**, *106* (6), 2065–2091. https://doi.org/10.1021/cr040109f.

(56) Chattaraj, P. K.; Giri, S.; Duley, S. Update 2 of: Electrophilicity Index. *Chem. Rev.* **2011**, *111* (2), PR43–PR75. https://doi.org/10.1021/cr100149p.

(57) Li, F.; Lu, J.; Ma, X. Metabolomic Screening and Identification of the Bioactivation Pathways of Ritonavir. *Chem. Res. Toxicol.* **2011**, *24* (12), 2109–2114. https://doi.org/10.1021/tx2004147.

(58) Lin, H.; D'Agostino, J.; Kenaan, C.; Calinski, D.; Hollenberg, P. F. The Effect of Ritonavir on Human CYP2B6 Catalytic Activity: Heme Modification Contributes to the Mechanism-Based Inactivation of CYP2B6 and CYP3A4 by Ritonavir. *Drug Metab. Dispos.* **2013**, *41* (10), 1813–1824. https://doi.org/10.1124/dmd.113.053108.

(59) Xu, L.; Liu, H.; Murray, B. P.; Callebaut, C.; Lee, M. S.; Hong, A.; Strickley, R. G.; Tsai, L. K.; Stray, K. M.; Wang, Y.; Rhodes, G. R.; Desai, M. C. Cobicistat (GS-9350): A Potent and Selective Inhibitor of Human CYP3A as a Novel Pharmacoenhancer. *ACS Med. Chem. Lett.* **2010**, *1* (5), 209–213. https://doi.org/10.1021/ml1000257.

(60) Pelletier, R. D. Selectivity and Mechanisms of Human Cytochrome P450 Inhibition by Chlormethiazole, 2019. https://doi.org/https://digital.lib.washington.edu/researchworks/handle/1773/45235.

(61) Offen, C. P.; Frearson, M. J.; Wilson, K.; Burnett, D. 4,5-Dimethylthiazole- N -Oxide- S -Oxide: A Metabolite of Chlormethiazole in Man. *Xenobiotica* **1985**, *15* (6), 503–511. https://doi.org/10.3109/00498258509045024.

(62) Ramesh, M.; Bharatam, P. V. Importance of Hydrophobic Parameters in Identifying Appropriate Pose of CYP Substrates in Cytochromes. *Eur. J. Med. Chem.* **2014**, *71*, 15–23. https://doi.org/10.1016/j.ejmech.2013.10.023.

(63) Jaladanki, C. K.; Shaikh, A.; Bharatam, P. V. Biotransformation of Isoniazid by Cytochromes P450: Analyzing the Molecular Mechanism Using Density Functional Theory. *Chem. Res. Toxicol.* **2017**, *30* (11), 2060–2073. https://doi.org/10.1021/acs.chemrestox.7b00129.

(64) Kumar, D.; Derat, E.; Khenkin, A. M.; Neumann, R.; Shaik, S. The High-Valent Iron-Oxo Species of

Polyoxometalate, If It Can Be Made, Will Be a Highly Potent Catalyst for C-H Hydroxylation and Double-Bond Epoxidation. *J. Am. Chem. Soc.* **2005**, *127* (50), 17712–17718. https://doi.org/10.1021/ja0542340.

(65) Kumar, D.; Karamzadeh, B.; Sastry, G. N.; de Visser, S. P. What Factors Influence the Rate Constant of Substrate Epoxidation by Compound I of Cytochrome P450 and Analogous Iron(IV)-Oxo Oxidants? *J. Am. Chem. Soc.* **2010**, *132* (22), 7656–7667. https://doi.org/10.1021/ja9106176.

(66) Shaik, S.; de Visser, S. P.; Ogliaro, F.; Schwarz, H.; Schröder, D. Two-State Reactivity Mechanisms of Hydroxylation and Epoxidation by Cytochrome P-450 Revealed by Theory. *Curr. Opin. Chem. Biol.* **2002**, *6* (5), 556–567. https://doi.org/10.1016/S1367-5931(02)00363-0.

(67) de Visser, S. P.; Ogliaro, F.; Shaik, S. How Does Ethene Inactivate Cytochrome P450 En Route to Its Epoxidation? A Density Functional Study. *Angew. Chemie Int. Ed.* **2001**, *40* (15), 2871–2874. https://doi.org/10.1002/1521-3773(20010803)40:15<2871::AID-ANIE2871>3.0.CO;2-R.

(68) Kumar, D.; Tahsini, L.; de Visser, S. P.; Kang, H. Y.; Kim, S. J.; Nam, W. Effect of Porphyrin Ligands on the Regioselective Dehydrogenation versus Epoxidation of Olefins by Oxoiron(IV) Mimics of Cytochrome P450. *J. Phys. Chem. A* **2009**, *113* (43), 11713–11722. https://doi.org/10.1021/jp9028694.

(69) Rydberg, P.; Jørgensen, F. S.; Olsen, L. Use of Density Functional Theory in Drug Metabolism Studies. *Expert Opin. Drug Metab. Toxicol.* **2014**, *10* (2), 215–227. https://doi.org/10.1517/17425255.2014.864278.

(70) Stare, J.; Henson, N. J.; Eckert, J. Mechanistic Aspects of Propene Epoxidation by Hydrogen Peroxide. Catalytic Role of Water Molecules, External Electric Field, and Zeolite Framework of TS-1. *J. Chem. Inf. Model.* **2009**, *49* (4), 833–846. https://doi.org/10.1021/ci800227n.

(71) McEwen, B. S. In Pursuit of Resilience: Stress, Epigenetics, and Brain Plasticity. *Ann. N. Y. Acad. Sci.* **2016**, *1373* (1), 56–64. https://doi.org/10.1111/nyas.13020.

(72) Lonsdale, R.; Harvey, J. N.; Mulholland, A. J. Inclusion of Dispersion Effects Significantly Improves Accuracy of Calculated Reaction Barriers for Cytochrome P450 Catalyzed Reactions. *J. Phys. Chem. Lett.* **2010**, *1* (21), 3232–3237. https://doi.org/10.1021/jz101279n.

(73) Dansette, P. M.; Bertho, G.; Mansuy, D. First Evidence That Cytochrome P450 May Catalyze Both S-Oxidation and Epoxidation of Thiophene Derivatives. *Biochem. Biophys. Res. Commun.* **2005**, *338* (1), 450–455. https://doi.org/http://dx.doi.org/10.1016/j.bbrc.2005.08.091.

(74) Chen, W.; Caceres-Cortes, J.; Zhang, H.; Zhang, D.; Humphreys, W. G.; Gan, J. Bioactivation of Substituted Thiophenes Including α-Chlorothiophene-Containing Compounds in Human Liver Microsomes. *Chem. Res. Toxicol.* **2011**, *24* (5), 663–669. https://doi.org/10.1021/tx100386z.

(75) Dansette, P. M.; Thang, D. C.; Mansuy, H. E. A. D. Evidence for Thiophene-s-Oxide as a Primary Reactive Metabolite of Thiophene in Vivo: Formation of a Dihydrothiophene Sulfoxide Mercapturic Acid. *Biochem. Biophys. Res. Commun.* **1992**, *186* (3), 1624–1630. https://doi.org/10.1016/S0006-291X(05)81594-3.

(76) López-Garcia, M. P.; Dansette, P. M.; Mansuy, D. Thiophene Derivatives as New Mechanism-Based Inhibitors of Cytochromes P-450: Inactivation of Yeast-Expressed Human Liver Cytochrome P-450 2C9

by Tienilic Acid. *Biochemistry* **1994**, *33* (1), 166–175.

(77) Medower, C.; Wen, L.; Johnson, W. W. Cytochrome P450 Oxidation of the Thiophene-Containing Anticancer Drug 3-[(Quinolin-4-Ylmethyl)-Amino]-Thiophene-2-Carboxylic Acid (4-Trifluoromethoxy-Phenyl)-Amide to an Electrophilic Intermediate. *Chem. Res. Toxicol.* **2008**, *21* (8), 1570–1577. https://doi.org/10.1021/tx700430n.

(78) Mansuy, D. Molecular Structure and Hepatotoxicity: Compared Data about Two Closely Related Thiophene Compounds. *J. Hepatol.* **1997**, *26* (2), 22–25. https://doi.org/10.1016/S0168-8278(97)80493-X.

(79) Valadon, P.; Dansette, P. M.; Girault, J. P.; Amar, C.; Mansuy, D. Thiophene Sulfoxides as Reactive Metabolites: Formation upon Microsomal Oxidation of a 3-Aroylthiophene and Fate in the Presence of Nucleophiles in Vitro and in Vivo. *Chem. Res. Toxicol.* **1996**, *9* (8), 1403–1413. https://doi.org/10.1021/tx9601622.

(80) Graham, E. E.; Walsh, R. J.; Hirst, C. M.; Maggs, J. L.; Martin, S.; Wild, M. J.; Wilson, I. D.; Harding, J. R.; Kenna, J. G.; Peter, R. M.; Williams, D. P.; Park, B. K. Identification of the Thiophene Ring of Methapyrilene as a Novel Bioactivation-Dependent Hepatic Toxicophore. *J. Pharmacol. Exp. Ther.* **2008**, *326* (2), 657–671. https://doi.org/10.1124/jpet.107.135483.

(81) Peterson, L. A. Reactive Metabolites in the Biotransformation of Molecules Containing a Furan Ring. *Chem. Res. Toxicol.* **2013**, *26* (1), 6–25. https://doi.org/10.1021/tx3003824.

(82) Ho, P. C.; Saville, D. J.; Wanwimolruk, S. Inhibition of Human CYP3A4 Activity by Grapefruit Flavonoids, Furanocoumarins and Related Compounds. *J. Pharm. Pharm. Sci.* **2001**, *4* (3), 217–227.

(83) Thelingwani, R. S.; Zvada, S. P.; Dolgos, H.; Ungell, A. L. B.; Masimirembwa, C. M. In Vitro and in Silico Identification and Characterization of Thiabendazole as a Mechanism-Based Inhibitor of CYP1A2 and Simulation of Possible Pharmacokinetic Drug-Drug Interactions. *Drug Metab. Dispos.* **2009**, *37* (6), 1286–1294. https://doi.org/10.1124/dmd.108.024604.

(84) Hughes, T. B.; Miller, G. P.; Swamidass, S. J. Modeling Epoxidation of Drug-like Molecules with a Deep Machine Learning Network. *ACS Cent. Sci.* **2015**, *1* (4), 168–180. https://doi.org/10.1021/acscentsci.5b00131.

(85) de Visser, S. P.; Shaik, S. A Proton-Shuttle Mechanism Mediated by the Porphyrin in Benzene Hydroxylation by Cytochrome P450 Enzymes. *J. Am. Chem. Soc.* **2003**, *125* (24), 7413–7424. https://doi.org/10.1021/ja034142f.

(86) Rademacher, P. M.; Woods, C. M.; Huang, Q.; Szklarz, G. D.; Nelson, S. D. Differential Oxidation of Two Thiophene-Containing Regioisomers to Reactive Metabolites by Cytochrome P450 2C9. *Chem. Res. Toxicol.* **2012**, *25* (4), 895–903. https://doi.org/10.1021/tx200519d.

(87) Lai, W.; Shaik, S. Can Ferric-Superoxide Act as a Potential Oxidant in P450(Cam)? QM/MM Investigation of Hydroxylation, Epoxidation, and Sulfoxidation. *J. Am. Chem. Soc.* **2011**, *133* (14), 5444–5452. https://doi.org/10.1021/ja111376n.

(88) Hirao, H.; Kumar, D.; Thiel, W.; Shaik, S. Two States and Two More in the Mechanisms of Hydroxylation and Epoxidation by Cytochrome P450. *J. Am. Chem. Soc.* **2005**, *127* (37), 13007–13018.

https://doi.org/10.1021/ja053847+.

(89) de Visser, S. P.; Ogliaro, F.; Sharma, P. K.; Shaik, S. What Factors Affect the Regioselectivity of Oxidation by Cytochrome P450? A DFT Study of Allylic Hydroxylation and Double Bond Epoxidation in a Model Reaction. *J. Am. Chem. Soc.* **2002**, *124* (39), 11809–11826. https://doi.org/10.1021/ja026872d.

(90) Bach, R. D.; Glukhovtsev, M. N.; Canepa, C. Oxidation of Alkenes, Sulfides, Amines, and Phosphines with Peroxynitrous Acid: Comparison with Other Oxidants Such as Peroxyformic Acid and Dimethyldioxirane. *J. Am. Chem. Soc.* **1998**, *120* (4), 775–783. https://doi.org/10.1021/ja972518h.

(91) Bach, R. D.; Coddens, B. A.; McDouall, J. J. W.; Schlegel, H. B.; Davis, F. A. The Mechanism of Oxygen Transfer from an Oxaziridine to a Sulfide and a Sulfoxide: A Theoretical Study. *J. Org. Chem.* **1990**, *55* (10), 3325–3330. https://doi.org/10.1021/jo00297a062.

(92) Bach, R. D.; Dmitrenko, O.; Estévez, C. M. Chemical Behavior of the Biradicaloid (HO···ONO) Singlet States of Peroxynitrous Acid. The Oxidation of Hydrocarbons, Sulfides, and Selenides. *J. Am. Chem. Soc.* **2005**, *127* (9), 3140–3155. https://doi.org/10.1021/ja044245d.

(93) Bach, R. D.; Owensby, A. L.; Gonzalez, C.; Schlegel, H. B.; McDouall, J. J. W. Nature of the Transition Structure for Oxygen Atom Transfer from a Hydroperoxide. Theoretical Comparison between Water Oxide and Ammonia Oxide. *J. Am. Chem. Soc.* **1991**, *113* (16), 6001–6011. https://doi.org/10.1021/ja00016a012.

(94) Kumar, D.; de Visser, S. P.; Sharma, P. K.; Hirao, H.; Shaik, S. Sulfoxidation Mechanisms Catalyzed by Cytochrome P450 and Horseradish Peroxidase Models: Spin Selection Induced by the Ligand. *Biochemistry* **2005**, *44* (22), 8148–8158. https://doi.org/10.1021/bi050348c.

(95) Loew, G. H.; Chang, Y.-T. Theoretical Studies of the Oxidation of N- and S-Containing Compounds by Cytochrome P450. *Int. J. Quantum Chem.* **1993**, *48* (27), 815–826. https://doi.org/10.1002/qua.560480873.

(96) Sharma, P. K.; de Visser, S. P.; Shaik, S. Can a Single Oxidant with Two Spin States Masquerade as Two Different Oxidants? A Study of the Sulfoxidation Mechanism by Cytochrome P450. *J. Am. Chem. Soc.* **2003**, *125* (29), 8698–8699. https://doi.org/10.1021/ja035135u.

(97) Li, C.; Zhang, L.; Zhang, C.; Hirao, H.; Wu, W.; Shaik, S. Which Oxidant Is Really Responsible for Sulfur Oxidation by Cytochrome P450? *Angew. Chemie Int. Ed.* **2007**, *46* (43), 8168–8170. https://doi.org/10.1002/anie.200702867.

(98) Rydberg, P.; Ryde, U.; Olsen, L. Sulfoxide, Sulfur, and Nitrogen Oxidation and Dealkylation by Cytochrome P450. *J. Chem. Theory Comput.* **2008**, *4* (8), 1369–1377. https://doi.org/10.1021/ct800101v.

(99) Geletii, Y. V; Musaev, D. G.; Khavrutskii, L.; Hill, C. L. Peroxynitrite Reactions with Dimethylsulfide and Dimethylselenide: An Experimental Study. *J. Phys. Chem. A* **2003**, *108* (2), 289–294. https://doi.org/10.1021/jp035955t.

(100) Musaev, D. G.; Geletii, Y. V; Hill, C. L. Theoretical Studies of the Reaction Mechanisms of Dimethylsulfide and Dimethylselenide with Peroxynitrite. *J. Phys. Chem. A* **2003**, *107* (30), 5862–5873. https://doi.org/10.1021/jp035144p.

(101) Bach, R. D.; Dmitrenko, O.; Estévez, C. M. Theoretical Analysis of Peroxynitrous Acid: Characterization of Its Elusive Biradicaloid (HO···ONO) Singlet States. *J. Am. Chem. Soc.* **2003**, *125* (52), 16204–16205. https://doi.org/10.1021/ja038524x.

(102) Canepa, C.; Bach, R. D.; Dmitrenko, O. Neutral versus Charged Species in Enzyme Catalysis. Classical and Free Energy Barriers for Oxygen Atom Transfer from C4a-Hydroperoxyflavin to Dimethyl Sulfide. *J. Org. Chem.* **2002**, *67* (24), 8653–8661. https://doi.org/10.1021/jo0261597.

(103) Porro, C. S.; Sutcliffe, M. J.; de Visser, S. P. Quantum Mechanics/Molecular Mechanics Studies on the Sulfoxidation of Dimethyl Sulfide by Compound I and Compound 0 of Cytochrome P450: Which Is the Better Oxidant? *J. Phys. Chem. A* **2009**, *113* (43), 11635–11642. https://doi.org/10.1021/jp9023926.

(104) Shaik, S.; Wang, Y.; Chen, H.; Song, J.; Meir, R. Valence Bond Modelling and Density Functional Theory Calculations of Reactivity and Mechanism of Cytochrome P450 Enzymes: Thioether Sulfoxidation. *Faraday Discuss.* **2010**, *145*, 49–70. https://doi.org/10.1039/B906094D.

(105) Kumar, D.; Sastry, G. N.; de Visser, S. P. Effect of the Axial Ligand on Substrate Sulfoxidation Mediated by Iron(IV)-Oxo Porphyrin Cation Radical Oxidants. *Chemistry* **2011**, *17* (22), 6196–6205. https://doi.org/10.1002/chem.201003187.

(106) Shaik, S.; Kumar, D.; de Visser, S. P.; Altun, A.; Thiel, W. Theoretical Perspective on the Structure and Mechanism of Cytochrome P450 Enzymes. *Chem. Rev.* **2005**, *105* (6), 2279–2328. https://doi.org/10.1021/cr030722j.

(107) Rydberg, P.; Jørgensen, M. S.; Jacobsen, T. A.; Jacobsen, A. M.; Madsen, K. G.; Olsen, L. Nitrogen Inversion Barriers Affect the N-Oxidation of Tertiary Alkylamines by Cytochromes P450. *Angew. Chemie - Int. Ed.* **2013**, *52* (3), 993–997. https://doi.org/10.1002/anie.201206207.

(108) Li, C.; Wu, W.; Cho, K.-B.; Shaik, S. Oxidation of Tertiary Amines by Cytochrome P450-Kinetic Isotope Effect as a Spin-State Reactivity Probe. *Chem. - A Eur. J.* **2009**, *15* (34), 8492–8503. https://doi.org/10.1002/chem.200802215.

(109) Cho, K. Bin; Moreau, Y.; Kumar, D.; Rock, D. A.; Jones, J. P.; Shaik, S. Formation of the Active Species of Cytochrome P450 by Using Iodosylbenzene: A Case for Spin-Selective Reactivity. *Chem. - A Eur. J.* **2007**, *13* (14), 4103–4115. https://doi.org/10.1002/chem.200601704.

(110) Hirao, H.; Chuanprasit, P.; Cheong, Y. Y.; Wang, X. How Is a Metabolic Intermediate Formed in the Mechanism-Based Inactivation of Cytochrome P450 by Using 1,1-Dimethylhydrazine: Hydrogen Abstraction or Nitrogen Oxidation? *Chem. - A Eur. J.* **2013**, *19* (23), 7361–7369. https://doi.org/10.1002/chem.201300689.

(111) Rydberg, P.; Olsen, L. Do Two Different Reaction Mechanisms Contribute to the Hydroxylation of Primary Amines by Cytochrome P450? *J. Chem. Theory Comput.* **2011**, *7* (10), 3399–3404. https://doi.org/10.1021/ct200422p.

(112) Seger, S. T.; Rydberg, P.; Olsen, L. Mechanism of the N-Hydroxylation of Primary and Secondary Amines by Cytochrome P450. *Chem. Res. Toxicol.* **2015**, *28* (4), 597–603. https://doi.org/10.1021/tx500371a.

(113) Lonsdale, R.; Fort, R. M.; Rydberg, P.; Harvey, J. N.; Mulholland, A. J. Quantum Mechanics/Molecular

Mechanics Modeling of Drug Metabolism: Mexiletine N-Hydroxylation by Cytochrome P450 1A2. *Chem. Res. Toxicol.* **2016**, *29* (6), 963–971. https://doi.org/10.1021/acs.chemrestox.5b00514.

(114) Hirao, H.; Thellamurege, N.; Chuanprasit, P.; Xu, K. Importance of H-Abstraction in the Final Step of Nitrosoalkane Formation in the Mechanism-Based Inactivation of Cytochrome P450 by Amine-Containing Drugs. *Int. J. Mol. Sci.* **2013**, *14* (12), 24692–24705. https://doi.org/10.3390/ijms141224692.

(115) Sambasivarao, S. V. NIH Public Access. **2013**, *18* (9), 1199–1216. https://doi.org/10.1016/j.micinf.2011.07.011.Innate.

(116) Chuanprasit, P.; Goh, S. H.; Hirao, H. Benzyne Formation in the Mechanism-Based Inactivation of Cytochrome P450 by 1-Aminobenzotriazole and *N* -Benzyl-1-Aminobenzotriazole: Computational Insights. *ACS Catal.* **2015**, *5* (5), 2952–2960. https://doi.org/10.1021/acscatal.5b00423.

(117) Hirao, H.; Chuanprasit, P. An Attempt to Evaluate the Effect of Proton-Coupled Electron Transfer on the H-Abstraction Step of the Reaction between 1,1-Dimethylhydrazine and Cytochrome P450 Compound I. *Chem. Phys. Lett.* **2015**, *621*, 188–192. https://doi.org/10.1016/j.cplett.2014.12.027.

(118) Ji, L.; Schüürmann, G. Model and Mechanism: N-Hydroxylation of Primary Aromatic Amines by Cytochrome P450. *Angew. Chem. Int. Ed. Engl.* **2013**, *52* (2), 744–748. https://doi.org/10.1002/anie.201204116.

(119) Ripa, L.; Mee, C.; Sjö, P.; Shamovsky, I. Theoretical Studies of the Mechanism of N-Hydroxylation of Primary Aromatic Amines by Cytochrome P450 1A2: Radicaloid or Anionic? *Chem. Res. Toxicol.* **2014**, *27* (2), 265–278. https://doi.org/10.1021/tx400376u.

(120) Low, C. M.; Ulgen, M.; Gorrod, J. W. The Recognition of a Diarylimine as a Metabonate Produced during Incubation of N-Benzyl-4-Chloroaniline with Hepatic Microsomal Preparations. *J. Pharm. Pharmacol.* **1994**, *46* (7), 585–590. https://doi.org/7996388.

(121) Ju, W.; Yang, S.; Ansede, J. H.; Stephens, C. E.; Bridges, A. S.; Voyksner, R. D.; Ismail, M. A.; Boykin, D. W.; Tidwell, R. R.; Hall, J. E.; Wang, M. Z. CYP1A1 and CYP1B1-Mediated Biotransformation of the Antitrypanosomal Methamidoxime Prodrug DB844 Forms Novel Metabolites through Intramolecular Rearrangement. *J. Pharm. Sci.* **2014**, *103* (1), 337–349. https://doi.org/10.1002/jps.23765.

(122) De Vries, H.; Beijersbergen Van Henegouwen, G. M. J.; Wouters, P. J. H. H. Correlations between Phototoxicity of Some 7-Chloro-I,4-Benzodiazepines and Their (Photo)Chemical Properties. *Pharm. Weekbl.* **1983**, *5* (6), 302–307. https://doi.org/10.1007/BF02074859.

(123) Ulgen, M.; Yilmaz, F.; Unsalan, S.; Gorrod, J. W. Chemical and Metabolic Studies on N-Benzyl-Tert-Butylamine and Its Potential Metabolites. *Drug Metabol. Drug Interact.* **1995**, *12* (2), 131–144. https://doi.org/10.1515/DMDI.1995.12.2.131.

(124) Ulgen, M.; Gorrod, J. W. Metabolic and Chemical Studies on α,N-Diarylnitrones. *Drug Metabol. Drug Interact.* **1994**, *11* (3), 245–257. https://doi.org/10.1515/DMDI.1994.11.3.245.

(125) Ulgen, M.; Yilmaz, F.; Dogruer, D. S.; Sahin, M. F. The in Vitro Hepatic Microsomal Metabolism of Methyl 2-(2(3H)-Benzoxazolone-3-Yl)Acetate in Rats. *Drug Metabol.Drug Interact.* **1999**, *15* (2–3), 173–179.

(126) Chen, H.; Murray, J.; Kornberg, B.; Dethloff, L.; Rock, D.; Nikam, S.; Mutlib, A. E. Metabolism-

Dependent Mutagenicity of a Compound Containing a Piperazinyl Indazole Motif: Role of a Novel P450-Mediated Metabolic Reaction Involving a Putative Oxaziridine Intermediate. *Chem. Res. Toxicol.* **2006**, *19* (10), 1341–1350. https://doi.org/10.1021/tx050354+.

(127) Cornelissen, P. J. G.; Beijersbergen, G. M. J.; Henegouwen, V.; Mohn, G. R. Structure and Photobiological Activity of 7-Chloro-1,4-Benzodiazepines. Studies on the Phototoxic Effects of Chlordiazepoxide, Desmethylchlordiazepoxide and Demoxepam Using a Bacterial Indicator System. *Photochem. Photobiol.* **1980**, *32* (5), 653–659. https://doi.org/10.1111/j.1751-1097.1980.tb04035.x.

(128) Wang, C. Y.; Muraoka, K.; Bryan, G. T. Mutagenicity of Nitrofurans, Nitrothiophenes, Nitropyrroles, Nitroimidazole, Aminothiophenes, and Aminothiazoles in <Em>Salmonella Typhimurium</Em> *Cancer Res.* **1975**, *35* (12), 3611 LP – 3617.

(129) Seifried, H. E.; Seifried, R. M.; Clarke, J. J.; Junghans, T. B.; San, R. H. C. A Compilation of Two Decades of Mutagenicity Test Results with the Ames Salmonella Typhimurium and L5178Y Mouse Lymphoma Cell Mutation Assays †. *Chem. Res. Toxicol.* **2006**, *19* (5), 627–644. https://doi.org/10.1021/tx0503552.

(130) Cameron, T. P.; Hughes, T. J.; Kirby, P. E.; Palmer, K. A.; Fung, V. A.; Dunkel, V. C. Mutagenic Activity of 5 Thiazole Compounds in the Salmonella/Microsome and Mouse Lymphoma TK+/− Assays. *Mutat. Res. Toxicol.* **1985**, *155* (1–2), 17–25. https://doi.org/10.1016/0165-1218(85)90020-5.

(131) Barnette, D. A.; Schleiff, M. A.; Osborn, L. R.; Flynn, N.; Matlock, M.; Swamidass, S. J.; Miller, G. P. Dual Mechanisms Suppress Meloxicam Bioactivation Relative to Sudoxicam. *Toxicology* **2020**, *440*, 152478. https://doi.org/10.1016/j.tox.2020.152478.

(132) Davydov, R.; Perera, R.; Jin, S.; Yang, T.-C.; Bryson, T. A.; Sono, M.; Dawson, J. H.; Hoffman, B. M. Substrate Modulation of the Properties and Reactivity of the Oxy-Ferrous and Hydroperoxo-Ferric Intermediates of Cytochrome P450cam As Shown by Cryoreduction-EPR/ENDOR Spectroscopy. *J. Am. Chem. Soc.* **2005**, *127* (5), 1403–1413. https://doi.org/10.1021/ja045351i.

(133) Kathuria, D.; Chourasiya, S. S.; Mandal, S. K.; Chakraborti, A. K.; Beifuss, U.; Bharatam, P. V. Ring-Chain Isomerism in Conjugated Guanylhydrazones: Experimental and Theoretical Study. *Tetrahedron* **2018**, *74* (23), 2857–2864. https://doi.org/10.1016/j.tet.2018.04.042.

(134) Koen, Y. M.; Sarma, D.; Hajovsky, H.; Galeva, N. A.; Williams, T. D.; Staudinger, J. L.; Hanzlik, R. P. Protein Targets of Thioacetamide Metabolites in Rat Hepatocytes. *Chem Res Toxicol* **2013**, *26* (4), 564–574. https://doi.org/10.1021/tx400001x.

(135) Hajovsky, H.; Hu, G.; Koen, Y.; Sarma, D.; Cui, W.; Moore, D. S.; Staudinger, J. L.; Hanzlik, R. P. Metabolism and Toxicity of Thioacetamide and Thioacetamide S-Oxide in Rat Hepatocytes. *Chem. Res. Toxicol.* **2012**, *25* (9), 1955–1963. https://doi.org/10.1021/tx3002719.